UNIVERSITÀ DEGLI STUDI DI TORINO

Carbonic anhydrase XII is a new therapeutic target to overcome chemoresistance in cancer cells

Joanna Kopecka[1,*], Ivana Campia[1,*], Andrea Jacobs[2], Andreas P. Frei[2,3], Dario Ghigo[1], Bernd Wollscheid[2,3], Chiara Riganti[1]

[1]Department of Oncology, University of Torino, 10126 Torino, Italy

[2]Department of Biology, Institute of Molecular Systems Biology, Swiss Federal Institute of Technology (ETH) Zurich, 8093 Zurich, Switzerland

[3]Biomedical Proteomics Platform (BMPP), Department of Health Sciences and Technology, Swiss Federal Institute of Technology (ETH) Zurich, 8093 Zurich, Switzerland

[*]These authors have contributed equally to this work

Correspondence to:
Chiara Riganti, **e-mail:** chiara.riganti@unito.it

Keywords: chemoresistance, surfaceome, P-glycoprotein, carbonic anhydrase type XII

Received: September 09, 2014 ***Accepted:*** December 09, 2014 ***Published:*** February 18, 2015

ABSTRACT

Multidrug resistance (MDR) in cancer cells is a challenging phenomenon often associated with P-glycoprotein (Pgp) surface expression. Finding new ways to bypass Pgp-mediated MDR still remains a daunting challenge towards the successful treatment of malignant neoplasms such as colorectal cancer.

We applied the Cell Surface Capture technology to chemosensitive and chemoresistant human colon cancer to explore the cell surface proteome of Pgp-expressing cells in a discovery-driven fashion. Comparative quantitative analysis of identified cell surface glycoproteins revealed carbonic anhydrase type XII (CAXII) to be up-regulated on the surface of chemoresistant cells, similarly to Pgp. In cellular models showing an acquired MDR phenotype due to the selective pressure of chemotherapy, the progressive increase of the transcription factor hypoxia-inducible factor-1 alpha was paralleled by the simultaneous up-regulation of Pgp and CAXII. CAXII and Pgp physically interacted at the cell surface. CAXII silencing or pharmacological inhibition with acetazolamide decreased the ATPase activity of Pgp by altering the optimal pH at which Pgp operated and promoted chemosensitization to Pgp substrates in MDR cells.

We propose CAXII as a new secondary marker of the MDR phenotype that influences Pgp activity directly and can be used as a pharmacological target for MDR research and potential treatment.

INTRODUCTION

One of the main features of chemoresistant cancer cells is the high cell surface expression of ATP binding cassette (ABC) transporters, such as P-glycoprotein (Pgp/ABCB1), multidrug resistance (MDR) related proteins (MRPs/ABCCs) and breast cancer resistance protein (BCRP/ABCG2). These plasma membrane transporters enable the active transport of chemotherapeutic drugs into the extracellular space, ultimately reducing intracellular concentrations, cytotoxicity, and therapeutic success [1–3]. Pgp is one of the ABC transporters with the broadest spectrum of substrates, which include anthracyclines, taxanes, Vinca alkaloids, epipodophyllotoxins, topotecan, methotrexate, imatinib, dasatinib, lapatinib, gefitinib, sorafenib, and erlotinib. As a consequence, tumors overexpressing Pgp often exhibit a MDR phenotype and are difficult to eradicate by chemotherapy [1, 4].

In attempts to overcome chemoresistance, ABC transporters have been targeted with pharmacological inhibitors. However, such approaches have led to several therapeutic failures due to the widespread tissue distribution of ABC transporters. Moreover, since ABC transporters play critical functions in the physiological clearance of catabolites and xenobiotics [5–7], their pharmacological inhibition

produces toxicities *in vivo*. Thus, pharmacological targeting of other surface proteins that are selectively overexpressed in chemoresistant cells and modulate the activity of ABC transporters is a promising alternative approach.

Until now, only few studies have analyzed the surfaceome of chemoresistant cells [8, 9]. These studies have identified proteins that were overexpressed in MDR cells, such as CD44 [8], dihydropyridine receptor alpha 2 and laminin subunit alpha 5 [9]. These cell surface proteins could be of clinical utility as potential biomarkers predictive of chemoresistance and/or potential therapeutic targets. However, these proteins were not found to modulate the expression or activity of Pgp or other ABC transporters in MDR cells, making them unlikely targets for the suppression of the MDR phenotype.

Pgp activity is finely modulated by the plasma-membrane lipid composition and physicochemical parameters [10]. A considerable number of proteins have been reported to physically interact with Pgp, such as the E3 ubiquitin ligases RNF2 [11] and FBXO15 [12], the endoplasmic reticulum-associated chaperon calreticulin [13], the serine/threonine kinase Pim-1 [14], the estrogen receptor repressor prohibitin 2 [15], the transcription factor Myc [16], the surface molecules caveolin-1 [17] and CD4 [18], the BRCA2 and CDKN1A-interacting protein BCCP, the Target of Rapamycin complex 2 subunit MAPKAP1 [18], and the lysosomal-associated protein LAPTM4B-35 [19]. Among these interactors, caveolin-1 [17] and RNF2 [11] negatively modulate Pgp activity, whereas LAPTM-35 is the only protein that has been shown to increase Pgp activity [19].

Here, we applied the Cell Surface Capturing (CSC) technology to investigate the surfaceome of a Pgp-negative (chemosensitive) and Pgp-positive (chemoresistant) human colon cancer model system, with the goal to identify quantitative surfaceome changes indicative of chemoresistance. This analysis identified carbonic anhydrase type XII (CAXII; accession number O43570, UniProtKB; http://www.uniprot.org) as a protein with significantly higher expression on the surface of chemoresistant cells. Based on this finding, we investigated whether changes in CAXII cell surface abundance were able to induce and/or maintain the MDR phenotype and whether CAXII could potentially be exploited as therapeutic target to chemosensitize MDR cells.

RESULTS

CAXII shows a higher cell surface abundance in chemoresistant cells than in chemosensitive cells

CSC technology, which selectively tags and purifies cell surface exposed glycopeptides for analysis by mass spectrometry, enabled the identification of 380 cell surface residing glycoproteins from human chemosensitive colon cancer HT29 cells and human chemoresistant colon cancer HT29/dx cells. The functional classification of the identified proteins is shown in Figure 1A. The quantitative analysis of cell surface protein expression in HT29/dx and in HT29 cells is reported in Figure 1B and in Supplemental Table 1.

Among the ABC transporters detected on the surface of chemoresistant cells, ABCC1/MRP1 was more abundant on HT29/dx cells, and ABCC3/MRP3, ABCA1, ABCA2 showed lower expression levels. One of the proteins with highest relative expression in chemoresistant cells was CAXII, which was 16-fold more expressed in HT29/dx cells than in parental HT29 cells (Figure 1B and Supplemental Table 1). CAXII topology and identified glycopeptides are shown in Supplemental Figure 1. These data were confirmed by confocal microscopy analysis (Figure 2A) and by immunoblot analysis of biotinylated extracts from HT29 and HT29/dx cells (Figure 2B). Biotinylation assays confirmed that Pgp and MRP1 were more abundant on the surface of HT29/dx compared to HT29 cells (Figure 2B). The ratio of N-glycosylated to deglycosylated Pgp in plasma membrane extracts was about 1 in HT29/dx cells, whereas the ratio of N-glycosylated to deglycosylated MRP1 was higher than 1 (Supplemental Figure 2A and 2B).

The higher surface abundance level of CAXII was not due to differential trafficking, since intracellular pools of CAXII were also elevated in HT29/dx whole cell lysate (Figure 2C). This phenomenon was not specific to colon cancer cells and higher levels of CAXII were also found in chemoresistant lung cancer A549/dx cells compared to chemosensitive A549 cells (Figure 2C). Similarly, a comparison of U2-OS cells with corresponding doxorubicin-resistant clones (U2-OS/dx 30, U2-OS/dx 100, U2-OS/dx 580) revealed that CAXII levels also correlated with chemoresistance in these osteosarcoma cells (Figure 2C). All tested chemoresistant cell lines had higher expression of Pgp than the corresponding chemosensitive cells; HT29/dx and A549/dx cells also had higher levels of MRP1, which was undetectable in the chemoresistant osteosarcoma cells (Figure 2C). On the basis of these results, we found a strong direct correlation between CAXII and Pgp expression (Figure 2D); no correlation was found for CAXII and MRP1 expression (not shown). According to tissues expression data, CAXII and Pgp (Supplemental Figure 3 and 4), but not CAXII and MRP1 (Supplemental Figure 3 and 5), were expressed at similar levels in colon adenocarcinoma samples.

CAXII expression increases during the acquisition of chemoresistance, in parallel with the increase of HIF-1α and Pgp

The difference in CAXII protein expression between HT29 and HT29/dx cells was paralleled by a striking difference in mRNA levels (Figure 3A). Upstream regulatory regions of the *CAXII* gene contain hypoxia-response element (HRE) sequences [20], suggesting that the

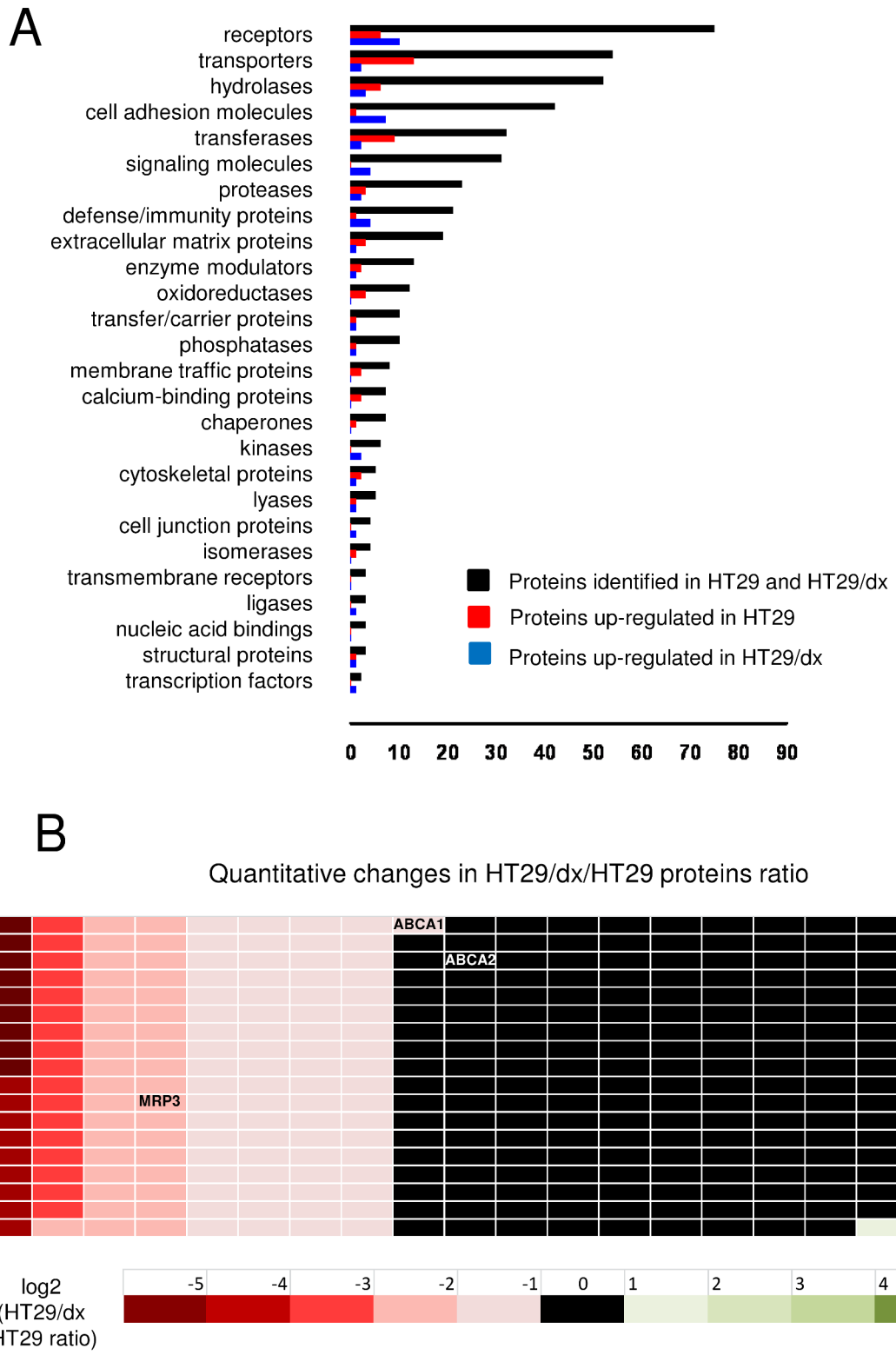

Figure 1: CSC technology enables the identification and quantitative comparison of the surface glycoproteome of human chemosensitive and chemoresistant colon cancer cells. (A) 380 identified plasma membrane-associated proteins (black bars) from human chemosensitive colon cancer HT29 cells and human chemoresistant colon cancer HT29/dx cells were categorized according to the biological function assigned by the PANTHER algorithm. **(B)** Quantitative analysis of the proteins detected by CSC technology. The ratio between protein expressed in HT29/dx cells and protein expressed in HT29 cells is represented by a colorimetric logarithmic scale. CAXII, ABCC1/MRP1, ABCC3/MRP3, ABCA1 and ABCA2 hits are indicated.

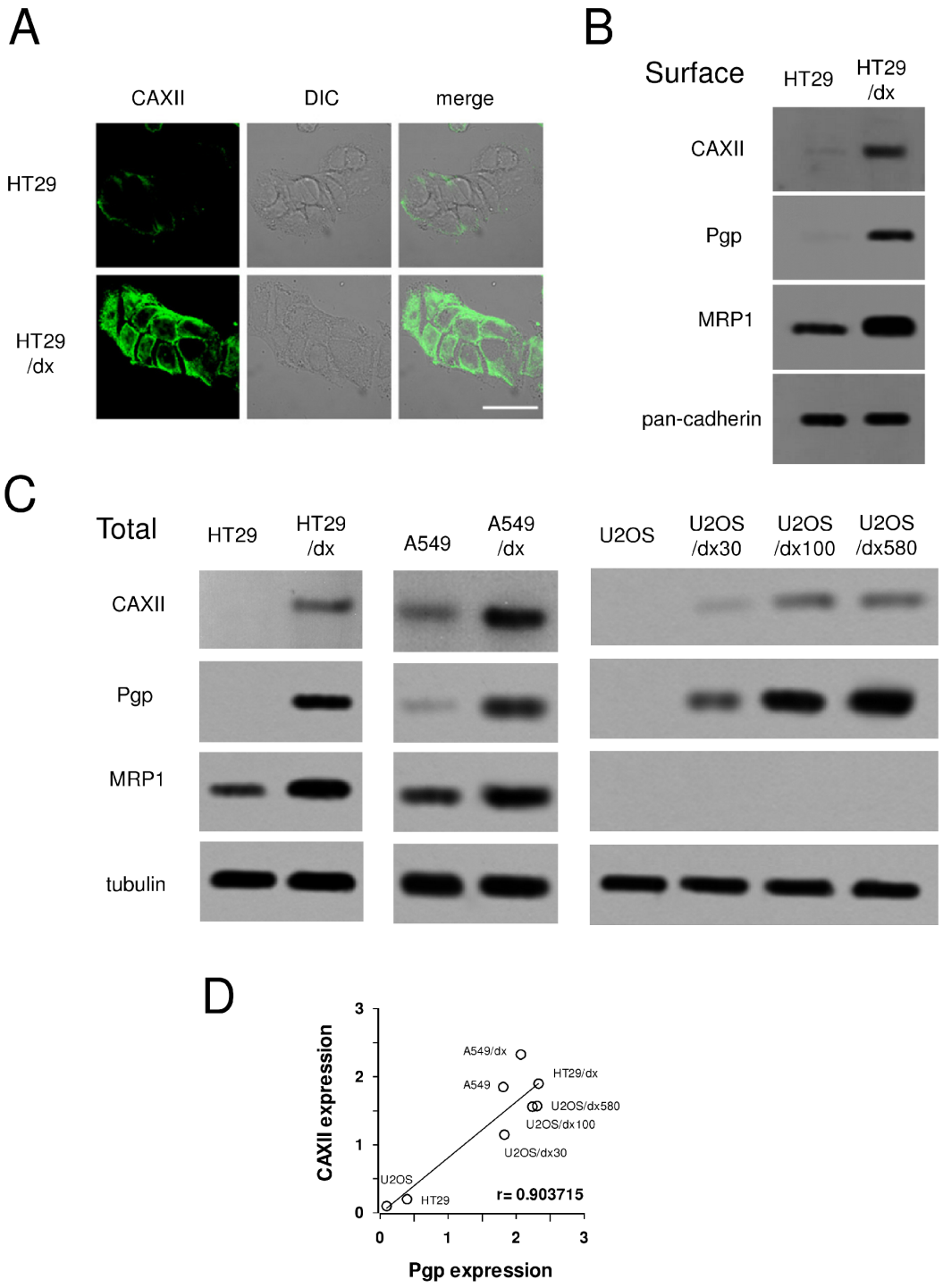

Figure 2: Expression of CAXII in chemosensitive and chemoresistant human cancer cells. Human chemosensitive colon cancer HT29 cells and their chemoresistant counterpart HT29/dx cells, human chemosensitive lung cancer A549 cells and their chemoresistant counterpart A549/dx cells, human chemosensitive osteosarcoma U2-OS cells and the chemoresistant clones U2-OS/dx 30, U2-OS/dx 100, U2-OS/dx 580 were subjected to the following assays. **(A)** Confocal microscope analysis of HT29 and HT29/dx cells stained for CAXII. The samples were analyzed by laser scanning confocal microscope for green fluorescence signal (CAXII) or by Nomarski differential interference contrast (DIC) optics. Magnification: 60 × objective; 10 × ocular lens. Bar = 20 μm. **(B)** Western blot analysis of biotinylated plasma membrane associated CAXII, Pgp and MRP1 in HT29 and HT29/dx cells. The pan-cadherin expression was used as a control of equal protein loading. The figure is representative of three experiments with similar results. **(C)** Whole cell lysates were analyzed by Western blotting for the expression of CAXII, Pgp and MRP1. The β-tubulin expression was used as a control of equal protein loading. The figure is representative of three experiments with similar results. **(D)** Linear regression analysis between CAXII and Pgp expression. The mean band density of CAXII and Pgp (panel C), expressed as arbitrary units, was calculated by ImageJ software (http://www.rsb.info.nih.gov/ij/). r coefficient was calculated using Fig. P software (Fig. P Software Inc., Hamilton, Canada).

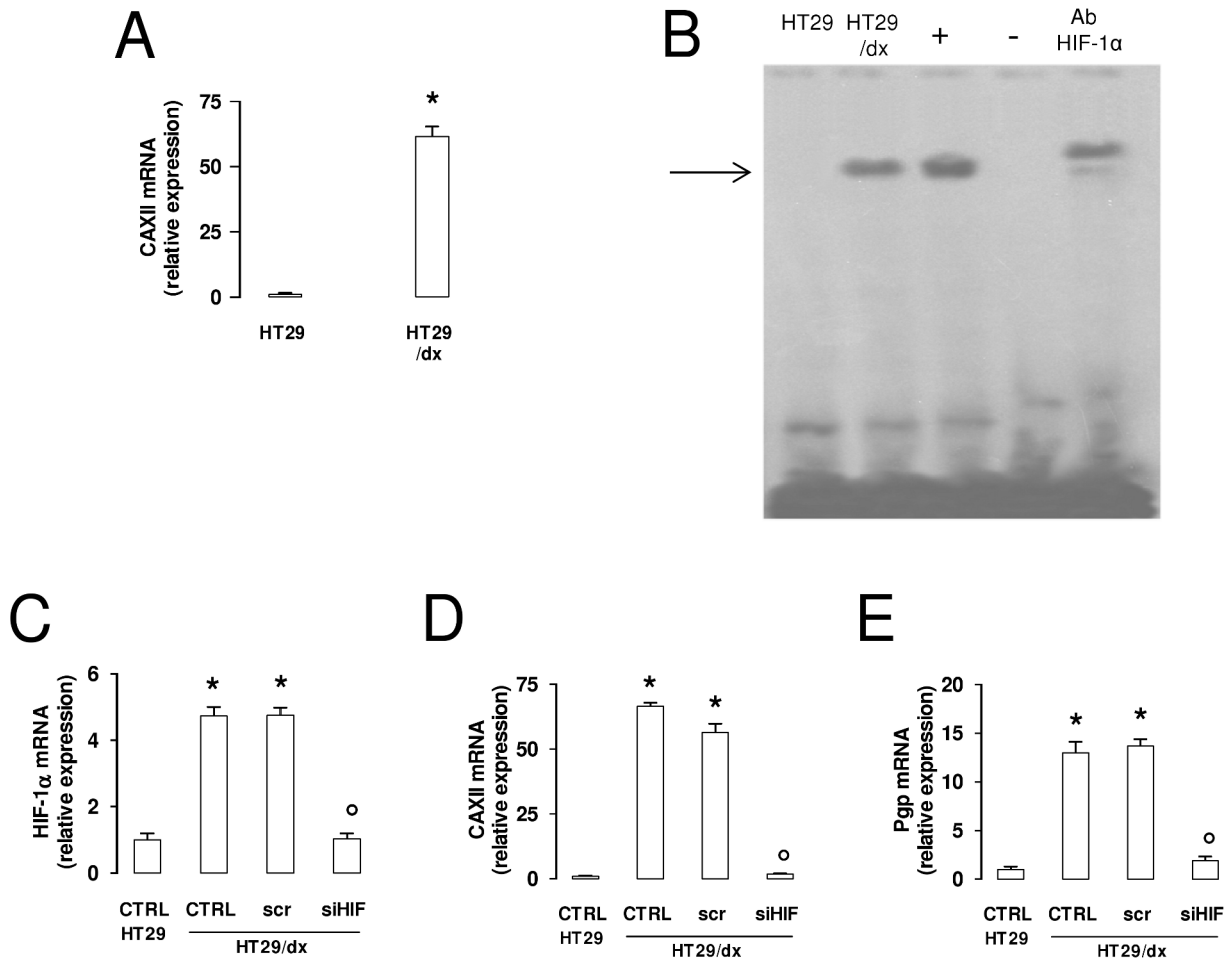

Figure 3: CAXII and Pgp expression levels are affected by HIF-1α in chemoresistant cells. (A) The *CAXII* mRNA level in HT29 and HT29/dx cells was detected by qRT-PCR. Data are presented as means ± SD ($n = 4$). Versus HT29: $*p < 0.001$. **(B)** EMSA detection of HIF-1α bound to its DNA consensus sequence was performed on nuclear extracts of normoxic HT29 and HT29/dx cells. Hypoxic HT29 cells (grown at 2% O_2 for 24 h) were used as positive control of HIF-1α activation (+). One lane was loaded with distilled water in place of cell extracts and was used as negative control (−). As control of specificity, the nuclear extracts of hypoxic HT29 cells were incubated with an anti-HIF-1α antibody (Ab HIF-1α). The band corresponding to the HIF-1α-DNA complex is indicated by the arrow. The figure is representative of three experiments with similar results. **(C–E)** mRNA was extracted from wild-type HT29 cells and HT29/dx cells (CTRL), HT29/dx cells treated with a non targeting scrambled siRNA (scr) or with a HIF-1α-targeting specific siRNA pool (siHIF) for 24 h. The expression of *HIF-1α* (panel **C**), *CAXII* (panel **D**) and *Pgp* (panel **E**) was detected by qRT-PCR. Data are presented as means ± SD ($n = 4$). Versus CTRL HT29: $*p < 0.001$; versus CTRL HT29/dx: $° p < 0.001$.

transcription factor hypoxia inducible factor-1α (HIF-1α) might be involved in the control of CAXII expression. HIF-1α activity was undetectable in HT29 cells, but present in HT29/dx where the protein was bound to HRE-containing DNA probes even under normoxic conditions (Figure 3B). In the chemoresistant cells, this leads to increased transcription of HIF-1α target genes, such as glucose transporter 1, hexokinase, aldolase-A, glyceraldehyde 3-phosphate dehydrogenase, phosphoglycerate kinase, enolase-A, lactate dehydrogenase, vascular endothelial growth factor, erythropoietin in the chemoresistant cells (Supplemental Figure 6). Moreover, HT29/dx cells had significantly higher levels of *HIF-1α* mRNA, together with increased levels of *CAXII* and *Pgp* mRNA, a known target gene of HIF-1α [21], than HT29 cells (Figure 3C–3E). Interestingly, *HIF-1α* silencing in HT29/dx cells (Figure 3C) produced a strong reduction of both *CAXII* (Figure 3D) and *Pgp* mRNA (Figure 3E), without affecting cell proliferation, apoptosis and viability of these cells (not shown).

The selection of chemoresistant cells from parental chemosensitive HT29 cells with increasing concentrations of doxorubicin induced a progressive increase of *HIF-1α* mRNA, measured every 5 passages of cell culture during the selection process (Figure 4A). The observed HIF-1α increase was paralleled by the progressive increase in *CAXII* (Figure 4B) and *Pgp* (Figure 4C) mRNA, and by the progressive decrease in the accumulation of doxorubicin (Figure 4D), a substrate of Pgp.

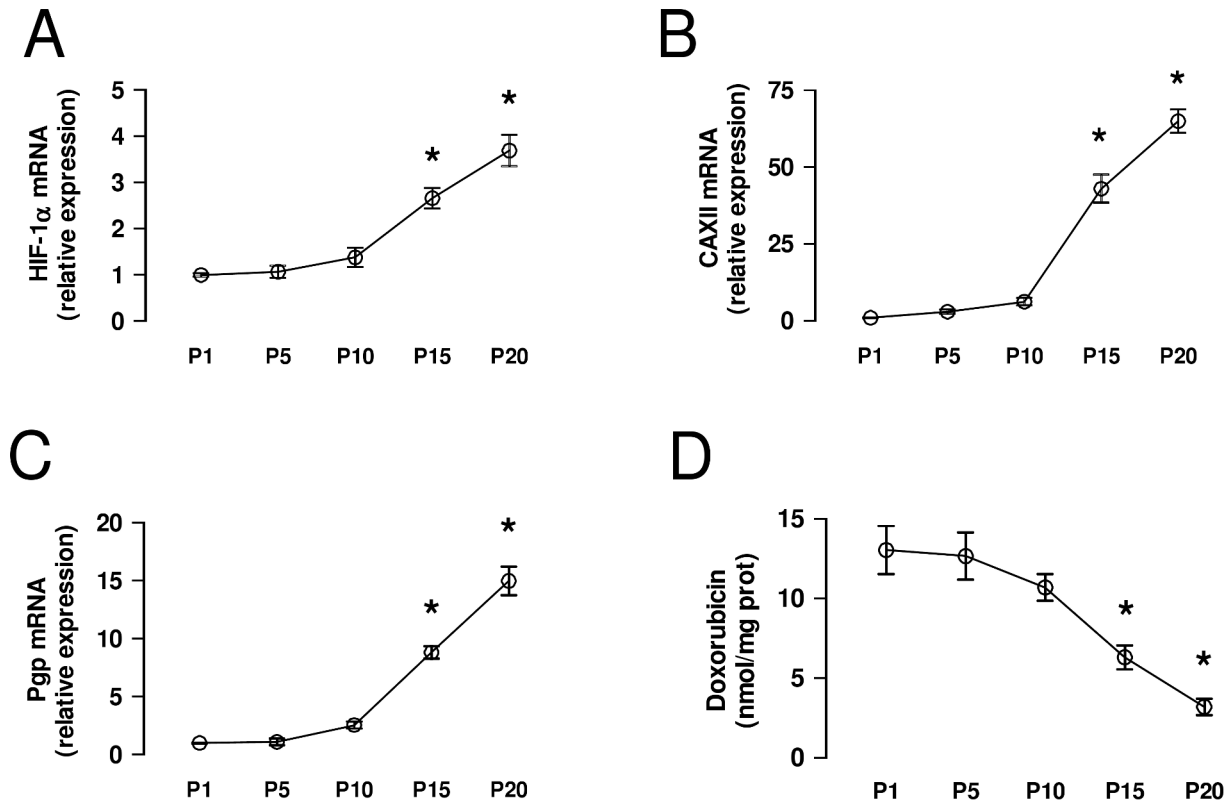

Figure 4: CAXII increases during the acquisition of chemoresistance. HT29 cells were cultured in medium containing increasing concentrations of doxorubicin, as detailed under Methods. **(A–C)** At passage *(P)* 1, 5, 10, 15, 20 the mRNA was extracted and the expression of *HIF-1α* (panel **A**), *CAXII* (panel **B**) and *Pgp* (panel **C**) was detected by qRT-PCR. Data are presented as means ± SD ($n = 4$). Versus P1: $*p < 0.001$. **(D)** An aliquot of cells was incubated 24 h with 5 μmol/L doxorubicin, then lysed and analyzed for the intracellular doxorubicin content. Data are presented as means ± SD ($n = 4$). Versus P1: $*p < 0.001$.

Depletion of CAXII does not affect proliferation and survival of chemoresistant cells

To investigate the functional role of CAXII in chemoresistant cells, we produced a HT29/dx subclone silenced for CAXII (Figure 5A). HT29 and HT29/dx cells did not show any appreciable difference in terms of: cell proliferation, as revealed by the proportion of Ki67-positive cells (Figure 5B); spontaneous apoptotic cell death, as indicated by the percentage of annexin V-fluorescein isothiocyanate (FITC)/propidium iodide (PI)-positive cells (Figure 5C); autophagy, as indicated by the expression level of classical autophagic markers such as beclin, ATG12 and LC3B (Figure 5D). Interestingly, untreated HT29/dx cells appeared more senescent than parental HT29 cells, as suggested by higher staining with β-galactosidase (Figure 5E). Despite the documented role of CAXII as a pro-oncogenic factor [22], enzyme silencing did not alter any of these parameters in chemoresistant cells (Figure 5B–5E).

CAXII is associated with Pgp and is necessary to maintain Pgp-mediated chemoresistance

Confocal microscope analysis showed that CAXII and Pgp co-localized on HT29/dx cells plasma membrane (Figure 6A). In co-immunoprecipitation assays, we found that CAXII was physically associated with Pgp, but not with MRP1 on HT29/dx cells plasma membrane (Figure 6B). CAXII co-immunoprecipitated with both glycosylated and deglycosylated Pgp (Supplemental Figure 7A). In some cell lines deglycosylated Pgp is less active, but in HT29/dx the glycosylation status of Pgp did not affect its ATPase activity (Supplemental Figure 7B).

These observations raised the question whether CAXII directly affected the activity of Pgp. Supporting this hypothesis, CAXII silencing in HT29/dx cells led to a dramatic decrease in Pgp ATPase activity (Figure 6C). As expected, HT29/dx cells accumulated significantly less doxorubicin than HT29 cells. In contrast, CAXII-silenced HT29/dx cells showed significantly increased levels of intracellular doxorubicin, reaching the same amount measured in HT29 cells (Figure 6D), where Pgp was undetectable (Figure 2C). In keeping with the different expression levels of Pgp, chemotherapeutic drugs that are substrates of Pgp, such as doxorubicin and irinotecan [23], reduced cell viability of HT29 cells, but not HT29/dx cells. However, both doxorubicin and irinotecan exhibited cytotoxic effects on HT29/dx cells silenced for CAXII (Figure 6E).

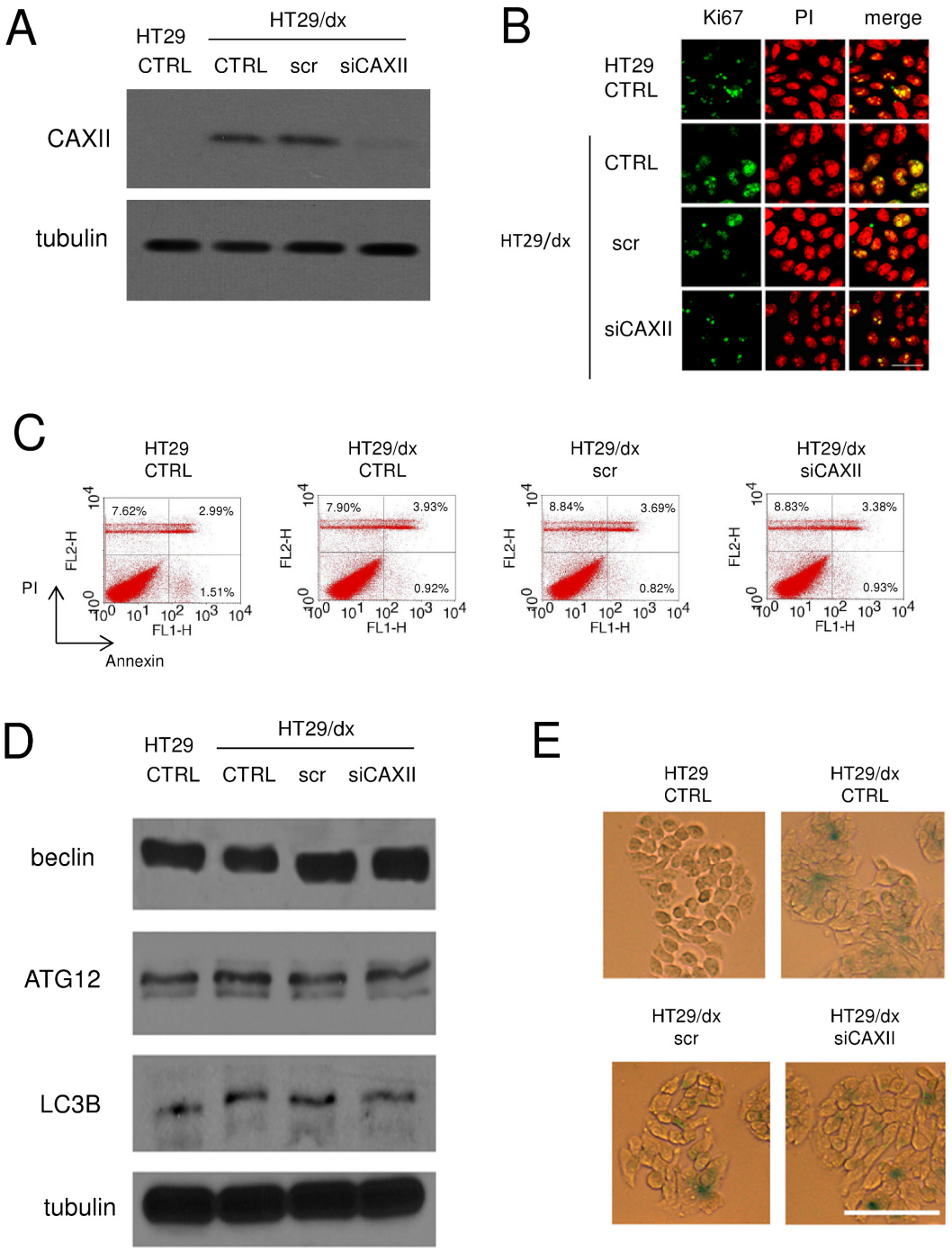

Figure 5: Depletion of CAXII does not affect proliferation and survival of chemoresistant cells. HT29/dx cells were cultured for 48 h with fresh medium (CTRL), treated with a non targeting scrambled siRNA (scr) or with a CAXII-targeting specific siRNA pool (siCAXII). HT29 cells were included as control. **(A)** The expression of CAXII was measured in whole cell lysates by Western blotting. The β-tubulin expression was used as a control of equal protein loading. The figure is representative of three experiments with similar results. **(B)** Confocal microscope analysis of cells stained for the proliferation marker Ki67. The samples were analyzed by laser scanning confocal microscopy for Ki67 protein signal (green fluorescence) or for PI (red fluorescence), used to visualize nuclei. Magnification: 60 × objective; 10 × ocular lens. Bar = 20 μm. **(C)** The percentage of cells positive to annexin V-FITC, as index of early apoptosis, and to PI, as index of late apoptosis, was measured by flow cytometry. Percentages indicate annexin V-positive cells (lower right quadrant), PI-positive cells (upper left quadrant), annexin V/PI-positive cells (upper right quadrant). The figures are representative of three experiments with similar results. **(D)** Western blot analysis of the autophagy markers beclin, ATG12 and LC3B. The β-tubulin expression was used as a control of equal protein loading. The figure is representative of three experiments with similar results. **(E)** Cells were fixed and stained for β-galactosidase activity, then examined by fluorescence microscopy. Magnification: 20 × objective; 10 × ocular lens. Bar = 100 μm.

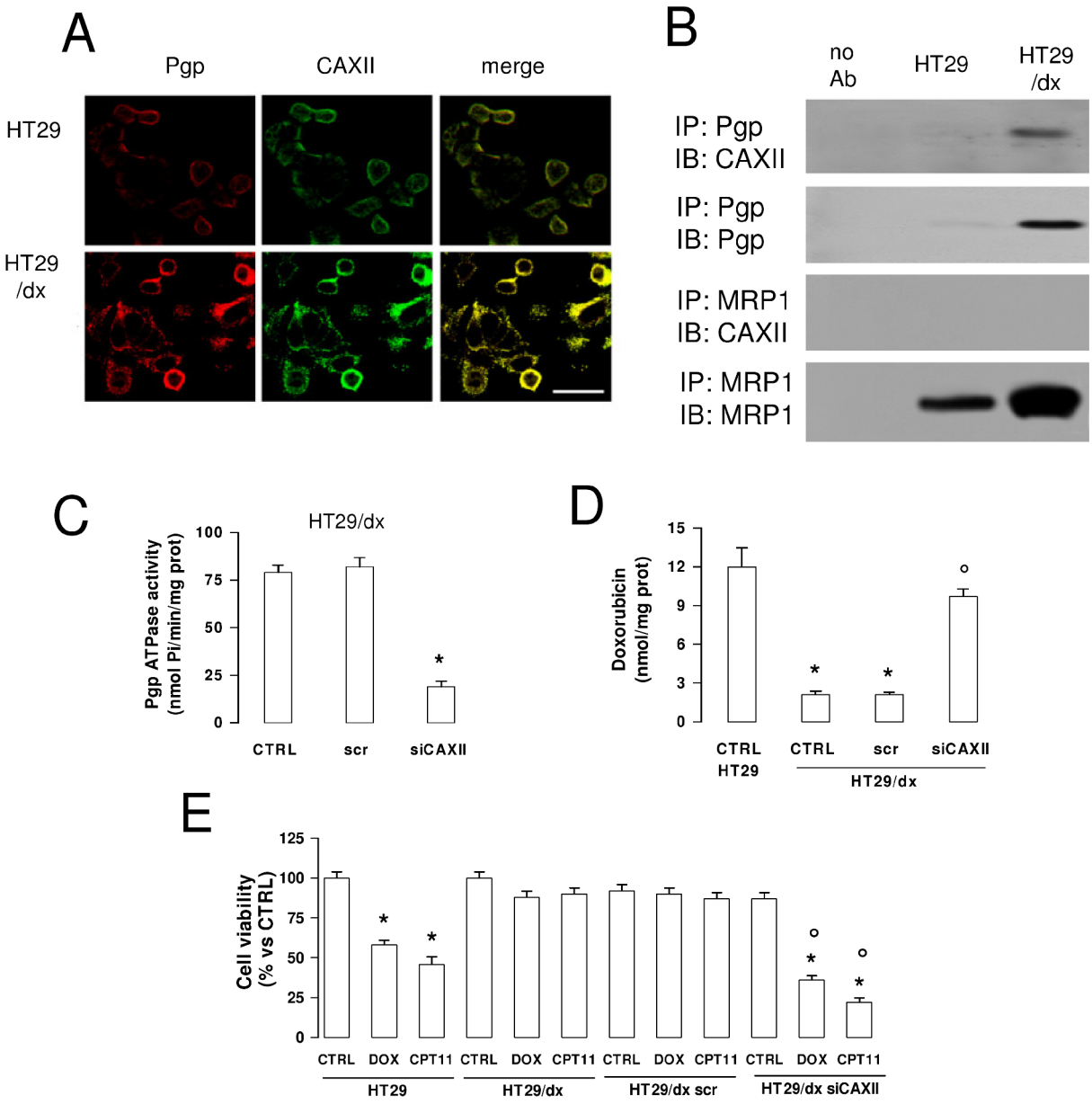

Figure 6: CAXII is physically associated with Pgp and increases Pgp activity in chemoresistant cells. **(A)** Confocal microscope analysis of HT29 and HT29/dx cells stained for CAXII and Pgp. The samples were analyzed by laser scanning confocal microscope for green (CAXII) or red (Pgp) fluorescence signal. Magnification: 60 × objective; 10 × ocular lens. Bar = 20 μm. **(B)** Biotinylated plasma membrane-derived extracts from HT29 and HT29/dx cells were immunoprecipitated (IP) with anti-Pgp or anti-MRP1 antibodies, then immunoblotted (IB) with anti-CAXII, anti-Pgp or anti-MRP1 antibodies. no Ab: samples immunoprecipitated without antibody. The figure is representative of three experiments with similar results. **(C)** HT29/dx cells were cultured for 48 h with fresh medium (CTRL), treated with a non targeting scrambled siRNA (scr) or with a CAXII-targeting specific siRNA pool (siCAXII). The Pgp ATPase activity was measured spectrophotometrically on Pgp-rich vesicles extracted from membrane fractions. Data are presented as means ± SD ($n = 4$). Versus CTRL: $^{*}p < 0.001$. **(D)** Cells treated as reported in C were incubated for 24 h with 5 μmol/L doxorubicin, then the intracellular drug content was measured fluorimetrically. HT29 were included as control of chemosensitive cells. Data are presented as means ± SD ($n = 4$). Versus HT29 CTRL: $^{*}p < 0.001$; versus HT29/dx CTRL: $^{\circ}$ $p < 0.001$. **(E)** Cells treated as reported in C were grown for 72 h in fresh medium (CTRL), or in medium containing 5 μmol/L doxorubicin (DOX) or 1 μM irinotecan (CPT11), then stained with neutral red dye. The absorbance of viable cells was measured spectrophotometrically. Data are presented as means ± SD ($n = 4$). For HT29 and HT29/dx cells, versus CTRL: $^{*}p < 0.001$; for HT29/dx cells, versus wild type HT29/dx DOX or HT29/dx CPT11, respectively: $^{\circ}$ $p < 0.002$.

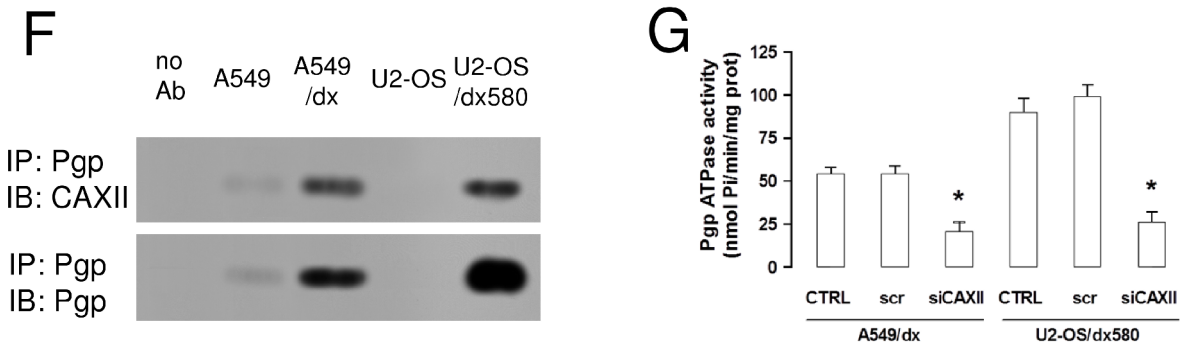

Figure 6: (*Continued*) (F) Biotinylated plasma membrane-derived extracts from human chemosensitive lung cancer A549 cell and chemoresistant A549/dx cells, human chemosensitive osteosarcoma U2-OS cells and chemoresistant U2-OS/dx580 cells were immunoprecipitated (IP) with an anti-Pgp antibody, then immunoblotted (IB) with an anti-CAXII or an anti-Pgp antibody. no Ab: samples immunoprecipitated without antibody. The figure is representative of two experiments with similar results. **(G)** A549/dx and U2-OS/dx580 cells were grown in fresh medium (CTRL), treated with a non targeting scrambled siRNA (scr) or with a CAXII-targeting specific siRNA pool (siCAXII). The Pgp ATPase activity was measured spectrophotometrically on Pgp-rich vesicles extracted from membrane fractions. Data are presented as means ± SD ($n = 3$). For both cell lines, versus CTRL: $*p < 0.001$.

The association between Pgp and CAXII was shared by other chemoresistant cells, such as lung cancer A549/dx cells and osteosarcoma resistant clones (Figure 6F). In analogy to HT29/dx cells, CAXII silencing (Supplemental Figure 8) reduced Pgp ATPase activity in these cell lines (Figure 6G).

CAIX is another isoform of carbonic anhydrase. This isoform is known to be highly expressed in tumors, including colon cancer, and has been linked to tumor aggressiveness and resistance to therapy [20]. This led us to investigate the expression levels of CAIX in our model system. In HT29 cells, *CAIX* mRNA levels were higher than the ones of *CAXII*, but were not increased in HT29/dx cells, where levels were significantly lower than for *CAXII* (Figure 7A). CAIX protein was detectable in HT29 and HT29/dx cells, without differences between chemosensitive and chemoresistant cells, both in whole cell lysates and in plasma membrane-derived extracts (Figure 7B). In contrast to CAXII (Figure 6B), CAIX did not co-immunoprecipitate with Pgp in plasma membrane extracts (Figure 7C). Moreover, CAIX-silenced HT29/dx cells (Figure 7D) retained the same low amount of intracellular doxorubicin than wild-type HT29/dx cells (Figure 7E), suggesting that CAIX is not involved in the chemosensitization towards Pgp substrates.

Pharmacological inhibition of CAXII restores chemosensitivity in chemoresistant cancer cells

Similarly to the effect of CAXII silencing, the CAXII inhibitor acetazolamide (Ki 5.6 ± 0.2 nM) [24] dose-dependently reduced the activity of Pgp (Figure 8A), suggesting that the activity of CAXII is critical for the catalytic activity of the transporter. At 1 μmol/L, acetazolamide, which was devoid of effects in HT29 cells where CAXII and Pgp were hardly detectable by Western blot (Figure 2B–2C), significantly increased the retention of doxorubicin (Figure 8B) and restored the cytotoxic effects of doxorubicin and irinotecan in HT29/dx cells (Figure 8C).

The activity of CAIX and CAXII has been reported to induce intracellular alkalinization [25]. As shown in Figure 8D, the pH_i of HT29 was 7.39 ± 0.02, whereas the pHi of HT29/dx was 7.58 ± 0.03. To investigate whether CAXII contributes to this different pHi between chemosensitive and chemoresistant cells, we measured the pHi in HT29/dx cells silenced for CAXII or treated with acetazolamide: interestingly, these experimental conditions lowered the pH_i of HT29/dx cells to values similar to HT29 cells. By contrast, acetazolamide did not affect the pH_i of low CAXII-expressing HT29 cells (Figure 8D). To evaluate whether such different pHi conditions may affect the activity of Pgp, we measured the ATPase activity of Pgp from HT29/dx plasma membrane in buffers with different pH. We did not detect changes in the basal ATPase activity of Pgp; by contrast, the verapamil-stimulated ATPase activity of Pgp, taken as an index of the transporter's maximal activity, increased from pH 7.0 to pH 7.6 (Figure 8E), suggesting that the optimal pH at which Pgp operates is slightly alkaline (i.e. compatible with the pH_i of HT29/dx cells) and that the pH produced by CAXII inhibition likely lowered Pgp activity.

DISCUSSION

In this work we analyzed the surfaceome of chemosensitive Pgp-negative and chemoresistant Pgp-positive human colon cancer cells and identified CAXII more highly expressed in the latter.

CAXII is a surface-associated enzyme highly expressed in tumors of renal [26], ovarian [27] and colorectal [28] origin, where it maintains the homeostasis of HCO_3^- [29].

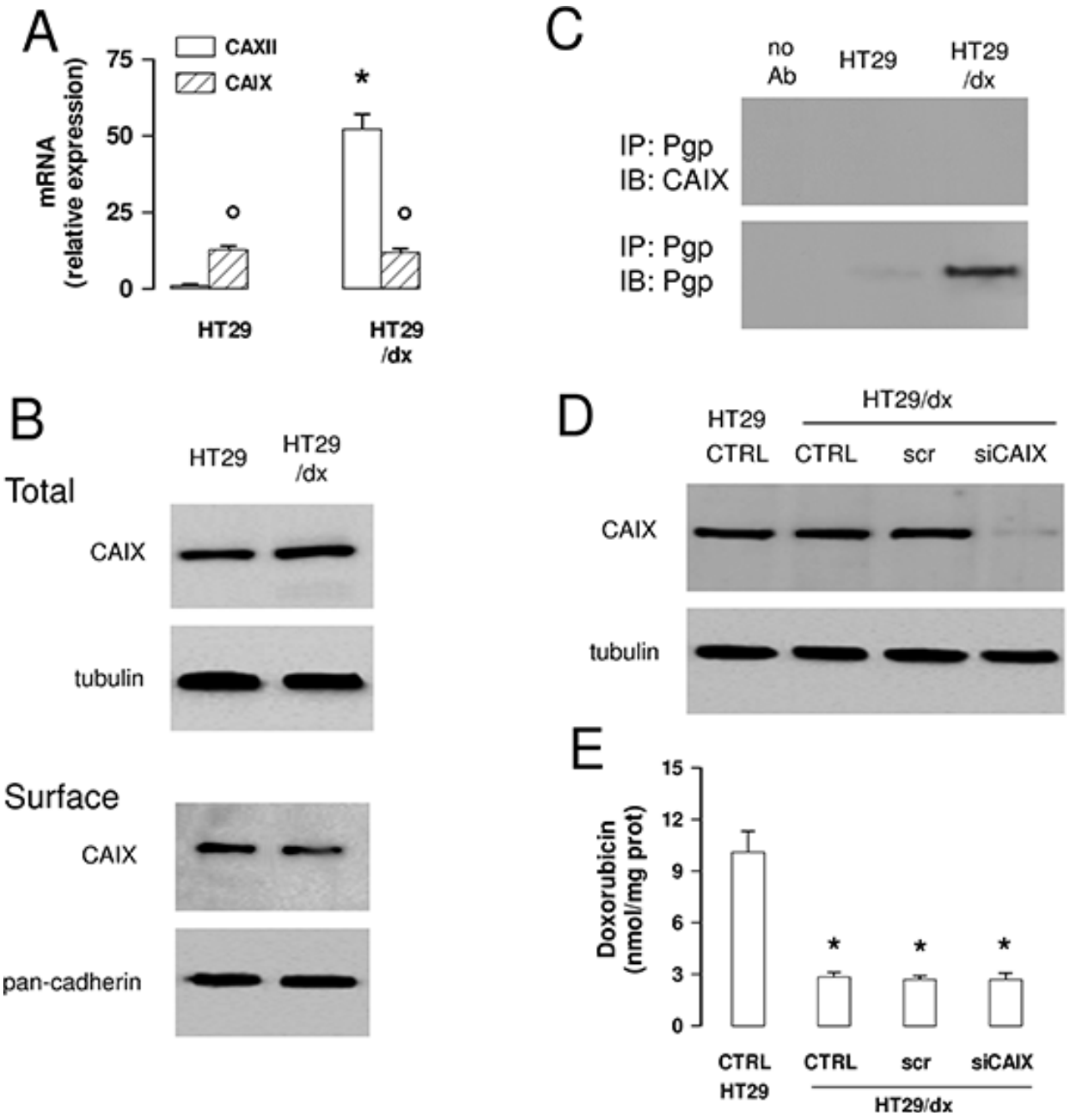

Figure 7: CAIX does not mediate chemoresistance to Pgp substrates in colon cancer cells. (A) The *CAIX* mRNA level in HT29 and HT29/dx cells was detected by qRT-PCR. *CAXII* mRNA level is shown for comparison. Data are presented as means ± SD (n = 4). Versus HT29: *$p < 0.001$; for both HT29 and HT29/dx cells, *CAIX* versus *CAXII* expression: ° $p < 0.001$. **(B)** Western blot analysis of CAIX expression in whole cell lysates (upper panel; Total) and biotinylated plasma membrane-derived extracts (lower panel; Surface) in HT29 and HT29/dx cells. The β-tubulin and pan-cadherin expression were used as controls of equal protein loading in whole cell lysates and plasma membrane-derived extracts, respectively. The figure is representative of three experiments with similar results. **(C)** Biotinylated plasma membrane-derived extracts from HT29 and HT29/dx cells were immunoprecipitated (IP) with an anti-Pgp antibody, then immunoblotted (IB) with an anti-CAIX or an anti-Pgp antibody. no Ab: samples immunoprecipitated without antibody. The figure is representative of three experiments with similar results. **(D)** HT29/dx cells were cultured for 48 h with fresh medium (CTRL), treated with a non targeting scrambled siRNA (scr) or with a CAIX-targeting specific siRNA pool (siCAIX). HT29 cells were included as control. The expression of CAIX was measured in whole cell lysates by Western blotting. The β-tubulin expression was used as a control of equal protein loading. The figure is representative of three experiments with similar results. **(E)** HT29/dx cells treated as reported in D were incubated for 24 h with 5 μmol/L doxorubicin, then the intracellular drug content was measured fluorimetrically. HT29 cells were included as control of chemosensitive cells. Data are presented as means ± SD (n = 4). Versus HT29 CTRL: *$p < 0.001$.

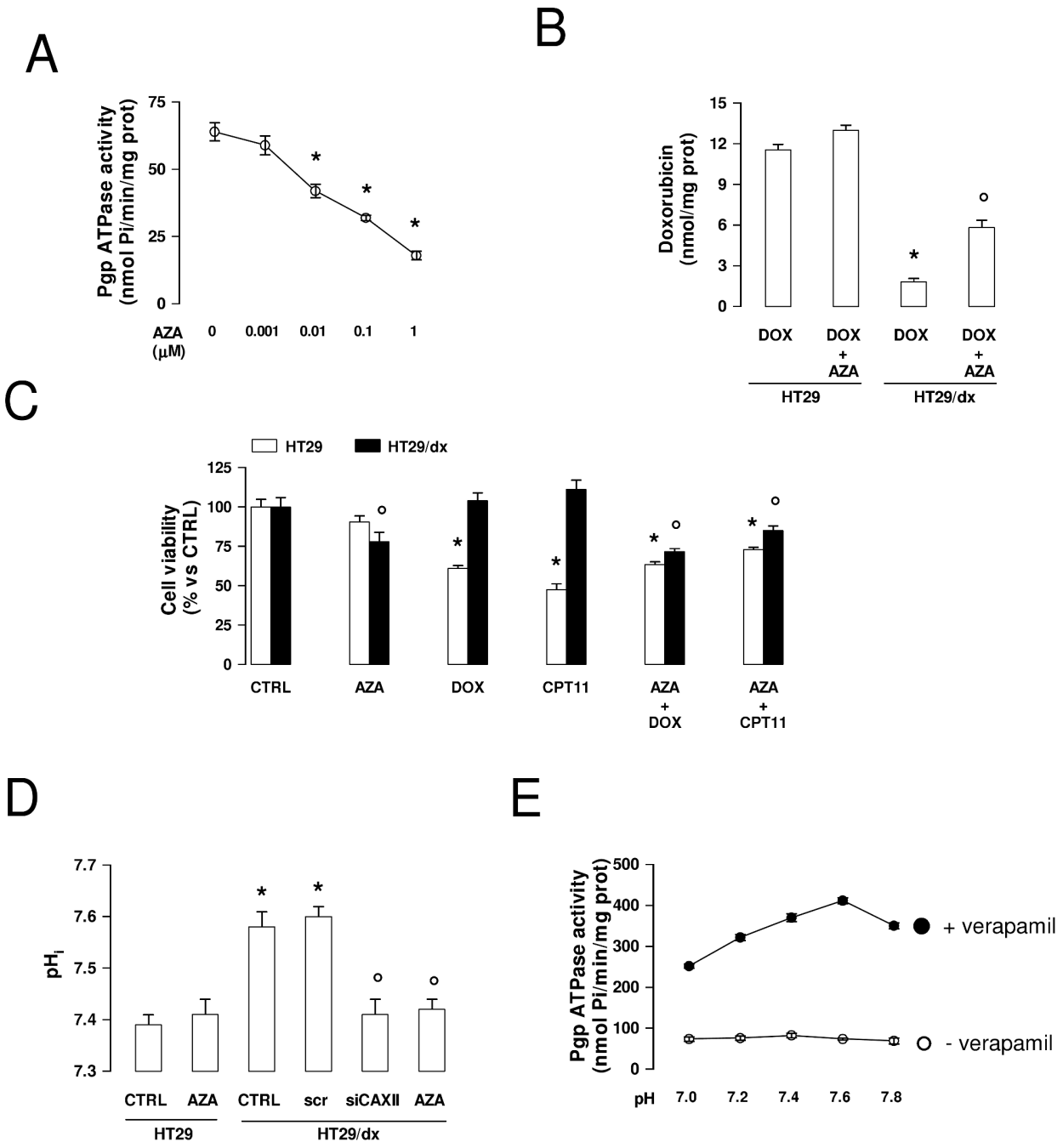

Figure 8: Effects of acetazolamide on Pgp activity, chemosensitivity and intracellular pH in chemoresistant cancer cells. (A) Pgp-rich vesicles were extracted from membrane fractions of HT29/dx cells, then the Pgp ATPase activity was measured spectrophotometrically in the absence (0) or in the presence of increasing concentrations of acetazolamide (AZA), added during the assay. Data are presented as means ± SD ($n = 4$). Versus 0: *$p < 0.005$. **(B)** HT29 and HT29/dx were incubated for 24 h with 5 μmol/L doxorubicin (DOX). When indicated, 1 μmol/L acetazolamide (AZA) was co-incubated. The intracellular doxorubicin retention was measured fluorimetrically. Data are presented as means ± SD ($n = 4$). HT29/dx DOX cells versus HT29 DOX cells: *$p < 0.001$; HT29/dx DOX+AZA cells versus HT29/dx DOX cells: ° $p < 0.005$. **(C)** Cells were grown for 72 h in fresh medium (CTRL), or in medium containing 1 μM acetazolamide (AZA), 5 μmol/L doxorubicin (DOX), 1 μM irinotecan (CPT11), alone or in combination, then stained with neutral red dye. The absorbance of viable cells was measured spectrophotometrically. Data are presented as means ± SD ($n = 4$). For HT29 cells, versus CTRL: *$p < 0.001$; for HT29/dx cells, versus CTRL: ° $p < 0.05$. **(D)** The intracellular pH (pH_i) measurement was performed in duplicate ($n = 4$) on HT29 and HT29/dx cells untreated or treated with a non targeting scrambled siRNA (scr), with a CAXII-targeting specific siRNA pool (siCAXII) for 48 h, with 1 μmol/L acetazolamide (AZA) for 24 h. Significance versus HT29 cells: *$p < 0.01$; versus HT29/dx cells: ° $p < 0.02$. **(E)** The Pgp ATPase activity was measured spectrophotometrically in Pgp-rich vesicles extracted from HT29/dx cell membrane fractions, using buffers with different pH, in the absence (open circles) or presence (solid circles) of 10 μmol/L verapamil, chosen as a Pgp activator. Data are presented as means ± SD ($n = 4$).

In our model of chemoresistant colon cancer cells, CAXII was increased at both the protein and mRNA level, suggesting that *CAXII* gene transcription was up-regulated. The presence of HRE sequences in upstream regions of the *CAXII* gene, and the down-regulation of *CAXII* mRNA in cells expressing the Von Hippel Lindau protein, a HIF-1α-inhibitor [20], led us to the hypothesis that HIF-1α might be involved in the control of CAXII expression. In HT29/dx cells, HIF-1α was constitutively active even under normoxia, as demonstrated by its constitutive binding of hypoxia-responsive DNA elements, and by higher expression levels of its classical target genes. This characteristic was progressively acquired during the selection of resistant clones from the parental chemosensitive population exposed to doxorubicin. Although we have previously reported the constitutive activation of HIF-1α in normoxic cancer cells with a stable MDR phenotype [30], the parallel increase in HIF-1α transcription and the progressive acquisition of MDR is a new observation. This trend may be due to the use of doxorubicin as selective agent: indeed, in normoxia the drug produces reactive oxygen species [31] that increase HIF-1α [32]. During the onset of the MDR phenotype, the increase of HIF-1α was paralleled by an increase of *CAXII* and *Pgp* mRNAs. These data suggest that HIF-1α may play a role in the up-regulation of CAXII in HT29/dx cells. Since the relative increase of *CAXII* mRNA was greater than for classical target genes of HIF-1α, other transcription factors and co-activators induced during the selection of chemoresistant clones – in addition to HIF-1α – are likely to be involved in the up-regulation of the *CAXII* gene.

In previous reports, CAXII overexpression has been associated with good [33, 34] or poor [35, 36] prognosis, depending on the tumor type. Furthermore, the protein has been reported to support cell proliferation and invasion, based on the observations that a monoclonal antibody against CAXII reduced tumor growth [22] and that CAXII inhibitors lowered metastatic potential [37] in mouse xenografts. However, according to the results obtained by CAXII silencing in HT29/dx cells, CAXII did not confer any selective advantage in terms of cell proliferation, spontaneous necrotic/apoptotic death, autophagy or senescence rate. By contrast, we found that CAXII promoted the acquisition and maintenance of chemoresistance.

In our study, Pgp and MRP1 were found to be up-regulated on the plasma membrane of HT29/dx cells. Whereas CSC technology successfully identified MRP1, it failed to identify Pgp. The gel shift of the MRP1 band upon treatment with Peptide-N-Glycosidase F (PNGase F) was bigger than the gel shift of the Pgp band, suggesting that the extent of glycosylation was higher in MRP1. This makes MRP1 easier to detect by CSC, which specifically identifies N-glycopeptides of cell surface proteins. Moreover, Pgp was highly abundant in its deglycosylated form in HT29/dx cells. Of note, CAXII was physically associated with both glycosylated and deglycosylated Pgp, which were equally active. We did not further investigate which domain of CAXII may be responsible for the interaction with Pgp. Pgp has a large intracellular domain (Supplemental Figure 9) and according to the crystal structure of CAXII, the intracellular C-terminal domain of the enzyme is likely to be responsible for the interactions with other proteins, the oligomerization of CAXII, the catalytic activity and the signal transduction [38].

In all chemoresistant cells tested in this study, CAXII appeared to support Pgp activity: CAXII-silenced cells showed a decreased ATPase activity of Pgp, an increased retention of the Pgp substrate doxorubicin, and a restored cytotoxicity of doxorubicin and irinotecan.

However, we cannot exclude that other tumor-associated CA isoforms are involved in the onset or maintenance of chemoresistance. For instance, the overexpression of CAIX has been correlated with a low response to doxorubicin treatment in breast cancer patients [39]. In our model, CAIX was expressed at similar levels in HT29 and HT29/dx cells. Furthermore, it seemed to play a minor role in the resistance to doxorubicin as illustrated by the fact that CAIX-silenced HT29/dx cells had the same low intracellular retention of doxorubicin than wild-type HT29/dx cells. What about the resistance phenotype?

It has previously been reported that the verapamil-stimulated activity of Pgp, considered an index of the maximal activity of the transporter, increases at slightly alkaline pH [40]. We confirmed this trend in Pgp-rich vesicles extracted from HT29/dx cells. The pH_i measured in HT29/dx cells was lowered by CAXII silencing or by pharmacological CAXII inhibition with acetazolamide, suggesting that CAXII may contribute to maintain the slightly alkaline pH_i of chemoresistant cells. A slightly alkaline pHi has been shown to induce resistance to doxorubicin in HT29/dx cells [41]. Furthermore, it has been reported that the activity of both CAIX and CAXII regulate the pHi homeostasis in cancer cells [25]. In our experiments, the selective silencing of CAIX and CAXII in HT29/dx cells suggested that only the latter was involved in the maintenance of doxorubicin resistance in this model. Since CAIX did not physically interact with Pgp, we hypothesize that it did not produce a sufficient alkalinization to reduce the transporter's efflux activity in the plasma membrane area where Pgp is localized. By contrast, the co-localization of Pgp and CAXII may favor the optimal pH condition for Pgp activity in the microenvironment where Pgp and CAXII are concentrated.

Our work shows that pharmacological inhibition of CAXII with acetazolamide effectively sensitizes resistant cells to the cytotoxic effects of Pgp substrates.

Acetazolamide has antitumor activity *in vivo* [42] and increases doxorubicin cytotoxicity in HT29 cells under hypoxia [43].

Since acetazolamide is being used in clinical practice as a diuretic, our work – although based on *in vitro* experiments – may have translational potential in the future. Given the role of CAXII in tumor growth and invasion, selective inhibitors of CAXII are under active development as new anticancer drugs [44–46], in particular against hypoxic tumors [47]. We propose that these synthetic and more selective inhibitors might be used as chemosensitizing agents for the treatment of Pgp overexpressing tumors. To achieve a more selective targeting of tumor cells, liposome- or nanoparticle-based carriers, which increase the intratumor accumulation of drugs, either by passive targeting (i.e. by the enhanced permeability retention effect) or active targeting [48], represent a valid approach. Our proteomic screening showed that, besides CAXII, a considerable number of other surface antigens were expressed at significantly higher levels in MDR cells. Some of these proteins may represent suitable targets for liposomes carrying CAXII inhibitors for the active and more selective targeting of chemoresistant colon cancer cells in preclinical models.

In summary, we show for the first time that CAXII is more highly abundant at the plasma membrane of Pgp-positive chemoresistant cells and is increased in parallel with Pgp during the acquisition of chemoresistance. Since CAXII activity is necessary for the optimal activity of Pgp, CAXII inhibitors may represent promising therapeutic tools to overcome Pgp-mediated chemoresistance.

METHODS

Chemicals

The plasticware for cell cultures was obtained from Falcon (Becton Dickinson, Franklin Lakes, NJ). The electrophoresis reagents were obtained from Bio-Rad Laboratories (Hercules, CA). The protein content of cell lysates was assessed with the BCA kit from Sigma Chemicals Co. (St. Louis, MO). Unless specified otherwise, all reagents were purchased from Sigma Chemicals Co.

Cells

Human chemosensitive colon cancer HT29 cells (from ATCC, Manassas, VA) were cultured in RPMI 1640 medium. A subpopulation, called HT29/dx, was created by culturing parental cells with 12.5 nmol/L doxorubicin for passages 1–5, 25 nmol/L doxorubicin for passages 6–10, 50 nmol/L doxorubicin for passages 11–15, 100 nmol/L doxorubicin for passages 16–20, then stably maintaining cells in RPMI 1640 medium containing 200 nmol/L doxorubicin. HT29-dx cells displayed a higher abundance of Pgp, MRP1 and BCRP, and were cross-resistant to doxorubicin and irinotecan [49]. Human chemosensitive lung cancer A549 cells (ATCC) and the chemoresistant A549/dx cell subline were obtained and cultured as reported [50]. Human doxorubicin sensitive osteosarcoma U2-OS cells and the corresponding clones with increasing resistance to doxorubicin (U2-OS/dx 30, U2-OS/dx 100, U2-OS/dx 580), selected by culturing U2-OS cells in a medium with 30, 100, 580 ng/mL doxorubicin, were a kind gift from Dr. Massimo Serra, Laboratory of Experimental Oncology (IRCCS Istituto Ortopedico Rizzoli, Bologna, Italy), and have been previously characterized [51].

Surface glycoprotein identification via CSC technology

Cells were prepared for CSC as described elsewhere [52]. Briefly, cells were treated for 15 min at 4°C in the dark with 2 mmol/L sodium meta-periodate (Thermo Fisher Scientific Inc., Waltham, MA) in PBS, pH 6.5, then washed and incubated with 6.5 mmol/L biocytin hydrazide (Biotium, Hayward, CA) in PBS, pH 6.5, for 1 h to biotinylate oxidized carbohydrates of cell surface glycoproteins. Cells were washed, incubated on ice in hypotonic lysis buffer (10 mmol/L Tris, 0.5 mmol/L $MgCl_2$, 10 mmol/L iodoacetamide, pH 7.5) for 10 min, homogenized for 10 s using a Dounce homogenizer. Afterward cell debris and nuclei were removed by centrifugation at 1 700 x g for 7 min. The supernatant was solubilized in 400 µL of digestion buffer (100 mmol/L NH_4HCO_3, 1 mmol/L iodoacetamide, 1 mmol/L 2,2′-thiodiethanol, 0.1% w/v RapiGest; Waters, Milan, Italy) and sonicated with a VialTweeter instrument (Hielscher Ultrasonic GmbH, Teltow, Germany). Proteins were digested overnight with trypsin in a protease:protein ratio of 1:100. After protein digestion, the peptide mixture was heated at 95°C for 10 min to inactivate trypsin, then biotinylated glycopeptides were bound to Streptavidin Plus UltraLink Resin (SA beads; Pierce, Rockford, IL) for 3 h at 37°C. After extensive washing, cysteine containing peptides, which were bound via a disulfide bridge to the biotinylated glycopeptides, were eluted from the SA beads by incubation with elution buffer (100 mmol/L NH_4HCO_3, 10 mmol/L tris(2-carboxyethyl)phosphine, 1 mmol/L dithiothreitol) for 1 h at room temperature. SA beads were washed again and N-linked glycopeptides were enzymatically released from the SA beads in a second overnight elution step in the presence of PNGase F. The free thiols of cysteine containing peptides were alkylated with iodoacetamide. Peptides were desalted on Ultra MicroTIP Columns (The Nest Group, Southborough, MA) and dried in a SpeedVac concentrator. Finally, peptides were solubilized in LC-MS grade water containing 0.1% v/v formic acid and 5% v/v acetonitrile.

MS/MS spectra were acquired with a LTQ Orbitrap XL mass spectrometer, converted to mzXML and searched against the UniProt database (Version 57.15) using the SEQUEST algorithm. Statistical data analysis was performed using a combination of ISB (Institute of Systems Biology, Seattle, WA) open-source software tools (PeptideProphetTM, ProteinProphetTM, TPP Version 4.3.1). A ProteinProphet probability score of at least 0.9 was used for data-filtering (corresponding to a false discovery rate of 1%). The protein functional classification was performed using the PANTHER algorithm (http://www.pantherdb.org). Quantitative data analysis was performed using the XPRESS software.

Western blot analysis

For whole cell lysates, the cells were rinsed with ice-cold lysis buffer (50 mmol/L Tris, 10 mmol/L EDTA, 1% v/v Triton-X100), supplemented with the protease inhibitor cocktail set III (80 μmol/L aprotinin, 5 mmol/L bestatin, 1.5 mmol/L leupeptin, 1 mmol/L pepstatin; Calbiochem, San Diego, CA), 2 mmol/L phenylmethylsulfonyl fluoride and 1 mmol/L Na_3VO_4, then sonicated and centrifuged at 13 000 x g for 10 min at 4°C. 20 μg protein extracts were subjected to SDS-PAGE and probed with the following antibodies: anti-CAXII (Abcam, Cambridge, UK); anti-CAIX (Novus Biologicals, Littleton, CO); anti-Pgp (C219, Calbiochem); anti-MRP1 (Abcam); anti-beclin (Abcam); anti-ATG12 (Abcam); anti-LC3B (Abcam); anti-β-tubulin (Santa Cruz Biotechnology Inc., Santa Cruz, CA), followed by a peroxidase-conjugated secondary antibody (Bio-Rad Laboratories). The membranes were washed with Tris-buffered saline-Tween 0.1% v/v, and the proteins were detected by enhanced chemiluminescence (Bio-Rad Laboratories). Plasma membrane-associated CAXII was evaluated in biotinylation assays, using the Cell Surface Protein isolation kit (Thermo Fisher Scientific Inc.), as previously reported [53], using an anti pan-cadherin antibody (Santa Cruz Biotechnology Inc.) to check the equal protein loading. In co-immunoprecipitation experiments, 100 μg of proteins were immunoprecipitated with the anti-Pgp or anti-MRP1 antibodies, using the PureProteome protein A and protein G Magnetic Beads (Millipore, Billerica, MA). The immunoprecipitated proteins were separated by SDS-PAGE and probed with the anti-CAXII, anti-CAIX, anti-Pgp or anti-MRP1 antibodies, followed by a peroxidase-conjugated secondary antibody. To detect glycosylated and deglycosyated proteins, biotinylated extracts (100 μg) were heated at 99°C for 10 min to denature proteins, then incubated for 1 h at 37°C in the absence or presence of 1 μU of human recombinant PNGaseF. Samples were resolved by SDS-PAGE and probed with the following antibodies, recognizing both the glycosylated and the deglycosylated forms: anti-Pgp (3C3.2, Millipore); anti-MRP1 (Enzo Life Sciences, Farmingdale, NY).

Confocal microscopy analysis

5×10^5 cells were grown on sterile glass coverslips, rinsed and fixed with 4% w/v paraformaldehyde for 15 min. To visualize surface CAXII and Pgp, the samples were washed with PBS and stained with an anti-CAXII antibody or an anti-Pgp antibody conjugated to phycoerythrin (Millipore) for 1 h. After washing, samples stained for CAXII were incubated with an AlexaFluor 488-conjugated secondary antibody (Millipore) for 1 h and re-washed. The coverslips were mounted with 4 μL of Gel Mount Aqueous Mounting and examined with an Olympus FV300 laser scanning confocal microscope (Olympus Biosystems, Tokyo, Japan). For each experimental point, a minimum of five microscopic fields were examined.

Quantitative real time-PCR (qRT-PCR)

Total RNA was extracted and reverse-transcribed using the QuantiTect Reverse Transcription Kit (Qiagen, Hilden, Germany). The qRT-PCR was performed with the IQ™ SYBR Green Supermix (Bio-Rad Laboratories). The same cDNA preparation was used to quantify the genes of interest and the housekeeping gene *S14*. The primer sequences, designed using the qPrimerDepot database (http://primerdepot.nci.nih.gov/), are reported in the Supplemental Table 2. The relative quantification was performed by comparing each PCR product with the housekeeping PCR product, using the Bio-Rad Software Gene Expression Quantitation (Bio-Rad Laboratories).

Electrophoretic mobility shift assay (EMSA)

Nuclear extracts were prepared as previously reported [54]. The probe containing the HIF-1α oligonucleotide consensus sequence was labeled with [γ-^{32}P]-ATP (3,000 Ci/μmol, 250 mCi; Amersham International, Little Chalfont, UK), using T4 polynucleotide kinase (Roche, Basel, Switzerland). Oligonucleotide sequence was 5′-TCTGTACGTGACCACACTCACCTC-3′. For each extract, 10 μg was incubated for 20 min with 20 000 cpm of [^{32}P]-labeled double-stranded oligonucleotide at 4°C. In the supershift assay, nuclear extracts were pre-incubated for 30 min at room temperature with 2 μL of an anti-HIF-1α antibody (Millipore); the reaction mixture containing the [^{32}P]-labeled double-stranded oligonucleotide was then added. The DNA-protein complex was separated on a non denaturating 4% polyacrylamide gel in TBE buffer (0.4 mol/L Tris, 0.45 mol/L boric acid, 0.5 mol/L EDTA, pH 8.0). After electrophoresis, the gel was dried and autoradiographed by exposure to X-ray film for 24 h.

Gene silencing

2×10^5 cells were transfected with 400 nmol/L of 20–25 nucleotide non targeting scrambled siRNA (Control siRNA-A, Santa Cruz Biotechnology Inc.) or

specific siRNA pools for CAXII, CAIX or HIF-1α (Santa Cruz Biotechnology Inc.), following the manufacturer's instructions. To verify the silencing efficacy, 24 h after the transfection the levels of mRNAs were checked by qRT-PCR, 48 h after the transfection the expression of proteins was checked by Western blotting. To verify the absence of cell toxicity after silencing, cell proliferation, apoptosis and viability was measured, as reported below.

Cell proliferation, apoptosis and senescence

To evaluate cell proliferation, 5×10^5 cells were grown on sterile glass coverslips, rinsed and fixed with 4% w/v paraformaldehyde for 15 min, then permeabilized with 0.1% v/v Triton-X100 for 5 min on ice, washed three times with PBS and stained with an anti-Ki67 antibody (Abcam) for 1 h at room temperature. After washing, samples were incubated with an AlexaFluor 488-conjugated secondary antibody (Millipore) for 1 h and re-washed. Finally, cells were stained with PI (1 μg/ml) to counterstain the nuclei, and washed again. The coverslips were mounted with 4 μL of Gel Mount Aqueous Mounting and examined by confocal microscopy as detailed above. Early and late apoptosis was measured by the Annexin V/Propidium Iodide Apoptosis Detection Kit (Sigma Chemical Co.). 1×10^5 cells were analyzed with a FACS-Calibur flow cytometer (Becton Dickinson). The percentage of cells positive to annexin V-FITC and PI was calculated with the Cell Quest software (Becton Dickinson). Cell senescence was evaluated on 5×10^5 cells fixed and stained with the Senescence Cells Histochemical Staining Kit (Sigma Chemical Co.), following the manufacturer's instruction. Samples were examined with a Leica DC100 fluorescence microscope (Leica Microsystems GmbH, Wetzlar, Germany). For each experimental point, a minimum of five microscopic fields were examined.

Intracellular doxorubicin accumulation

Doxorubicin content was measured fluorimetrically as detailed elsewhere [55]. The results were expressed as nmol doxorubicin/mg cell proteins, according to a titration curve previously set.

Cell viability

Cell viability was evaluated by measuring the percentage of cells stained with neutral red dye, as reported previously [49]. The viability of untreated cells was considered 100%; the results were expressed as percentage of viable cells in each experimental condition versus untreated cells.

ATPase Pgp activity

The assay was performed on Pgp-enriched membrane vesicles as detailed elsewhere [56]. Verapamil (10 μmol/L) was added to the reaction mix to achieve a maximal activation of the Pgp ATPase activity. Results were expressed as nmol hydrolyzed phosphate (Pi)/min/mg proteins, according to the titration curve previously prepared.

Intracellular pH (pH_i) measurement

The pHi was measured by incubating whole cells with 5 μmol/L of 2',7'-bis-(2-carboxyethyl)-5-(and-6)-carboxyfluorescein acetoxymethyl ester (BCECF-AM) for 15 min at 37°C and reading the intracellular fluorescence by a FACSCalibur flow cytometer (Becton Dickinson). The intracellular fluorescence was converted into pH units according to a titration curve, as described previously [41].

Statistical analysis

All data in text and figures are provided as means ± SD. The results were analyzed by a one-way Analysis of Variance (ANOVA). A $p < 0.05$ was considered significant.

ACKNOWLEDGEMENTS

This work was supported by grants from the Italian Association for Cancer Research (AIRC; grant MFAG 11475 and IG 15232), the Italian Ministry of University and Research ("Future in Research program" FIRB 2012, grant RBFR12SOQ1) to C.R.; the Swiss National Science Foundation (SNSF, 31003A_135805) to B.W.

JK is fellow of the Italian Foundation for Cancer Research (FIRC).

We thank Erika Ortolan (Department of Medical Sciences, University of Torino) and Costanzo Costamagna (Department of Oncology, University of Torino) for the technical assistance.

Conflict of interest

None.

REFERENCES

1. Gottesman MM, Fojo T, Bates SE. Multidrug resistance in cancer: role of ATP-dependent transporters. Nat Rev Cancer. 2002; 2:48–58.
2. Borst P, Evers R, Kool M, Wijnholds J. A family of drug transporters: the multidrug resistance-associated proteins. J Natl Cancer Inst. 2000; 92:1295–1302.
3. Polgar O, Bates SE. ABC transporters in the balance: is there a role in multidrug resistance? Biochem Soc Trans. 2005; 33:241–245.
4. Brózik A, Hegedüs C, Erdei Z, Hegedus T, Özvegy-Laczka C, Szakács G, Sarkadi B. Tyrosine kinase inhibitors as modulators of ATP binding cassette multidrug

transporters: substrates, chemosensitizers or inducers of acquired multidrug resistance? Expert Opin Drug Metab Toxicol. 2011; 7:623–642.

5. Sarkadi B, Homolya L, Szakács G, Váradi A. Human multidrug resistance ABCB and ABCG transporters: participation in a chemoimmunity defense system. Physiol Rev. 2006; 86:1179–1236.
6. Ueda K. ABC proteins protect the human body and maintain optimal health. Biosci Biotechnol Biochem. 2011; 75:401–409.
7. Zutz A, Gompf S, Schägger H, Tampé R. Mitochondrial ABC proteins in health and disease. Biochim Biophys Acta. 2009; 1787:681–690.
8. Cain JW, Hauptschein RS, Stewart JK, Bagci T, Sahagian GG, Jay DG. Identification of CD44 as a surface biomarker for drug resistance by surface proteome signature technology. Mol Cancer Res. 2011; 9:637–647.
9. Li K, Sun Z, Zheng J, Lu Y, Bian Y, Ye M, Wang X, Nie Y, Zou H, Fan D. In-depth research of multidrug resistance related cell surface glycoproteome in gastric cancer. J Proteomics. 2013; 82:130–140.
10. Sharom FJ. Complex Interplay between the P-Glycoprotein Multidrug Efflux Pump and the Membrane: Its Role in Modulating Protein Function. Front Oncol. 2014; 4:e41.
11. Rao PS, Mallya KB, Srivenugopal KS, Balaji KC, Rao US. RNF2 interacts with the linker region of the human P-glycoprotein. Int J Oncol. 2006; 29:1413–1419.
12. Katayama K, Noguchi K, Sugimoto Y. FBXO15 regulates P-glycoprotein/ABCB1 expression through the ubiquitin-proteasome pathway in cancer cells. Cancer Sci. 2013; 104:694–702.
13. Kopecka J, Campia I, Brusa D, Doublier S, Matera L, Ghigo D, Bosia A, Riganti C. Nitric oxide and P-glycoprotein modulate the phagocytosis of colon cancer cells. J Cell Mol Med. 2011; 15:1492–1504.
14. Xie Y, Burcu M, Linn DE, Qiu Y, Baer MR. Pim-1 kinase protects P-glycoprotein from degradation and enables its glycosylation and cell surface expression. Mol Pharmacol. 2010; 78:310–318.
15. Ewing RM, Chu P, Elisma F, Li H, Taylor P, Climie S, McBroom-Cerajewski L, Robinson MD, O'Connor L, Li M, Taylor R, Dharsee M, Ho Y, et al. Large-scale mapping of human protein-protein interactions by mass spectrometry. Mol Syst Biol. 2007; 3:e89.
16. Agrawal P, Yu K, Salomon AR, Sedivy JM. Proteomic profiling of Myc-associated proteins. Cell Cycle. 2010; 9:4908–4921.
17. Cai C, Chen J. Overexpression of caveolin-1 induces alteration of multidrug resistance in Hs578T breast adenocarcinoma cells. Int J Cancer. 2004; 111:522–529.
18. Wang J, Huo K, Ma L, Tang L, Li D, Huang X, Yuan Y, Li C, Wang W, Guan W, Chen H, Jin C, Wei J, et al. Toward an understanding of the protein interaction network of the human liver. Mol Syst Biol. 2011; 7:e536.
19. Li L, Wei XH, Pan YP, Li HC, Yang H, He QH, Pang Y, Shan Y, Xiong FX, Shao GZ, Zhou RL. LAPTM4B: a novel cancer-associated gene motivates multidrug resistance through efflux and activating PI3K/AKT signaling. Oncogene. 2010; 29:5785–5795.
20. Pastorekova S, Zatovicova M, Pastorek J. Cancer-associated carbonic anhydrases and their inhibition. Curr Pharm Des. 2008; 14:685–698.
21. Comerford KM, Wallace TJ, Karhausen J, Louis NA, Montalto MC, Colgan SP. Hypoxia-inducible factor-1-dependent regulation of the multidrug resistance (MDR1) gene. Cancer Res. 2002; 62:3387–3394.
22. Gondi G, Mysliwietz J, Hulikova A, Jen JP, Swietach P, Kremmer E, Zeidler R. Antitumor efficacy of a monoclonal antibody that inhibits the activity of cancer-associated carbonic anhydrase XII. Cancer Res. 2013; 73:6494–6503.
23. Luo F, Paranjpe PV, Guo A, Rubin E, Sinko P. Intestinal transport of irinotecan in Caco-2 cells and MDCK II cells overexpressing efflux transporters Pgp, cMOAT and MRP1. Drug Metab Dispos. 2002; 30:763–770.
24. Güzel-Akdemir Ö, Akdemir A, Isik S, Vullo D, Supuran CT. o-Benzenedisulfonimido-sulfonamides are potent inhibitors of the tumor-associated carbonic anhydrase isoforms CA, IX, and CA, XII. Bioorg Med Chem. 2013; 21:1386–1391.
25. Chiche J, Ilc K, Laferrière J, Trottier E, Dayan F, Mazure NM, Brahimi-Horn MC, Pouysségur J. Hypoxia-inducible carbonic anhydrase IX and XII promote tumor cell growth by counteracting acidosis through the regulation of the intracellular pH. Cancer Res. 2009; 69:358–368.
26. Rafalko A, Iliopoulos O, Fusaro VA, Hancock W, Hincapie M. Immunoaffinity enrichment and liquid chromatography-selected reaction monitoring mass spectrometry for quantitation of carbonic anhydrase 12 in cultured renal carcinoma cells. Anal Chem. 2010; 82:8998–9005.
27. Hynninen P, Vaskivuo L, Saarnio J, Haapasalo H, Kivelä J, Pastoreková S, Pastorek J, Waheed A, Sly WS, Puistola U, Parkkila S. Expression of transmembrane carbonic anhydrases IX and XII in ovarian tumours. Histopathology. 2006; 49:594–602.
28. Kivelä A, Parkkila S, Saarnio J, Karttunen TJ, Kivelä J, Parkkila AK, Waheed A, Sly WS, Grubb JH, Shah G, Türeci O, Rajaniemi H. Expression of a novel transmembrane carbonic anhydrase isozyme XII in normal human gut and colorectal tumors. Am J Pathol. 2000; 156:577–584.
29. Ulmasov B, Waheed A, Shah GN, Grubb JH, Sly WS, Tu C, Silverman DN. Purification and kinetic analysis of recombinant CA, XII, a membrane carbonic anhydrase overexpressed in certain cancers. Proc Natl Acad Sci USA. 2000; 97:14212–14217.
30. Riganti C, Castella B, Kopecka J, Campia I, Coscia M, Pescarmona G, Bosia A, Ghigo D, Massaia M. Zoledronic acid restores doxorubicin chemosensitivity and immunogenic cell death in multidrug-resistant human cancer cells. PLoS One. 2013; 8:e60975.

31. Deavall DG, Martin EA, Horner JM, Roberts R. Drug-induced oxidative stress and toxicity. J Toxicol. 2012; 2012:e645460.
32. Cho KH, Choi MJ, Jeong KJ, Kim JJ, Hwang MH, Shin SC, Park CG, Lee HY. A ROS/STAT3/HIF-1α signaling cascade mediates EGF-induced TWIST1 expression and prostate cancer cell invasion. Prostate. 2014; 74:528–536.
33. Watson PH, Chia SK, Wykoff CC, Han C, Leek RD, Sly WS, Gatter KC, Ratcliffe P, Harris AL. Carbonic anhydrase XII is a marker of good prognosis in invasive breast carcinoma. Br J Cancer. 2003; 88:1065–1070.
34. Ilie MI, Hofman V, Ortholan C, Ammadi RE, Bonnetaud C, Havet K, Venissac N, Mouroux J, Mazure NM, Pouysségur J, Hofman P. Overexpression of carbonic anhydrase XII in tissues from resectable non-small cell lung cancers is a biomarker of good prognosis. Int J Cancer. 2011; 128:1614–1623.
35. Haapasalo J, Hilvo M, Nordfors K, Haapasalo H, Parkkila S, Hyrskyluoto A, Rantala I, Waheed A, Sly WS, Pastorekova S, Pastorek J, Parkkila AK. Identification of an alternatively spliced isoform of carbonic anhydrase XII in diffusely infiltrating astrocytic gliomas. Neuro Oncol. 2008; 10:131–138.
36. Chien MH, Ying TH, Hsieh YH, Lin CH, Shih CH, Wei LH, Yang SF. Tumor-associated carbonic anhydrase XII is linked to the growth of primary oral squamous cell carcinoma and its poor prognosis. Oral Oncol. 2012; 48:417–423.
37. Gieling RG, Babur M, Mamnani L, Burrows N, Telfer BA, Carta F, Winum JY, Scozzafava A, Supuran CT, Williams KJ. Antimetastatic effect of sulfamate carbonic anhydrase IX inhibitors in breast carcinoma xenografts. J Med Chem. 2012; 55:5591–5600.
38. Whittington DA, Waheed A, Ulmasov B, Shah GN, Grubb JH, Sly WS, Christianson DW. Crystal structure of the dimeric extracellular domain of human carbonic anhydrase XII, a bitopic membrane protein overexpressed in certain cancer tumor cells. Proc Natl Acad Sci USA. 2001; 98:9545–9550.
39. Betof AS, Rabbani ZN, Hardee ME, Kim SJ, Broadwater G, Bentley RC, Snyder SA, Vujaskovic Z, Oosterwijk E, Harris LN, Horton JK, Dewhirst MW, Blackwell KL. Carbonic anhydrase IX is a predictive marker of doxorubicin resistance in early-stage breast cancer independent of HER2 and TOP2A amplification. Br J Cancer. 2012; 106:916–922.
40. Aänismaa P, Seelig A. P-Glycoprotein kinetics measured in plasma membrane vesicles and living cells. Biochemistry. 2007; 46:3394–3404.
41. Miraglia E, Viarisio D, Riganti C, Costamagna C, Ghigo D, Bosia A. Na^+/H^+ exchanger activity is increased in doxorubicin-resistant human colon cancer cells and its modulation modifies the sensitivity of the cells to doxorubicin. Int J Cancer. 2005; 115:924–929.
42. Ahlskog JK, Dumelin CE, Trüssel S, Mårlind J, Neri D. *In vivo* targeting of tumor-associated carbonic anhydrases using acetazolamide derivatives. Bioorg Med Chem Lett. 2009; 19:4851–4856.
43. Gieling RG, Parker CA, De Costa LA, Robertson N, Harris AL, Stratford IJ, Williams KJ. Inhibition of carbonic anhydrase activity modifies the toxicity of doxorubicin and melphalan in tumour cells *in vitro*. J Enzyme Inhib Med Chem. 2013; 28:360–369.
44. Salmon AJ, Williams ML, Wu QK, Morizzi J, Gregg D, Charman SA, Vullo D, Supuran CT, Poulsen SA. Metallocene-based inhibitors of cancer-associated carbonic anhydrase enzymes IX and XII. J Med Chem. 2012; 55:5506–5517.
45. Tars K, Vullo D, Kazaks A, Leitans J, Lends A, Grandane A, Zalubovskis R, Scozzafava A, Supuran CT. Sulfocoumarins (1,2-benzoxathiine-2,2-dioxides): a class of potent and isoform-selective inhibitors of tumor-associated carbonic anhydrases. J Med Chem. 2013; 56:293–300.
46. D'Ascenzio M, Carradori S, De Monte C, Secci D, Ceruso M, Supuran CT. Design, synthesis and evaluation of N-substituted saccharin derivatives as selective inhibitors of tumor-associated carbonic anhydrase XII. Bioorg Med Chem. 2014; 22:1821–1831.
47. Morris JC, Chiche J, Grellier C, Lopez M, Bornaghi LF, Maresca A, Supuran CT, Pouysségur J, Poulsen SA. Targeting hypoxic tumor cell viability with carbohydrate-based carbonic anhydrase IX and XII inhibitors. J Med Chem. 2011; 54:6905–6918.
48. Fonseca NA, Gregório AC, Valério-Fernandes A, Simões S, Moreira JN. Bridging cancer biology and the patients' needs with nanotechnology-based approaches. Cancer Treat Rev. 2014; 40:626–635.
49. Gelsomino G, Corsetto PA, Campia I, Montorfano G, Kopecka J, Castella B, Gazzano E, Ghigo D, Rizzo AM, Riganti C. Omega 3 fatty acids chemosensitize multidrug resistant colon cancer cells by down-regulating cholesterol synthesis and altering detergent resistant membranes composition. Mol Cancer. 2013; 12:e137.
50. Kopecka J, Campia I, Olivero P, Pescarmona G, Ghigo D, Bosia A, Riganti C. A LDL-masked liposomal-doxorubicin reverses drug resistance in human cancer cells. J Contr Rel. 2011; 149:196–205.
51. Serra M, Scotlandi K, Manara MC, Maurici D, Lollini PL, De Giovanni C, Toffoli G, Baldini N. Establishment and characterization of multidrug-resistant human osteosarcoma cell lines. Anticancer Res. 1993; 13:323–329.
52. Bausch-Fluck D, Hofmann A, Wollscheid B. Cell surface capturing technologies for the surfaceome discovery of hepatocytes. Methods Mol Biol. 2012; 909:1–16.
53. De Boo S, Kopecka J, Brusa D, Gazzano E, Matera L, Ghigo D, Bosia A, Riganti C. iNOS activity is necessary for the cytotoxic and immunogenic effects of doxorubicin in human colon cancer cells. Mol Cancer. 2009; 8:e108.

54. Campia I, Gazzano E, Pescarmona G, Ghigo D, Bosia A, Riganti C. Digoxin and ouabain increase the synthesis of cholesterol in human liver cells. Cell Mol Life Sci. 2009; 66:1580–1594.

55. Riganti C, Miraglia E, Viarisio D, Costamagna C, Pescarmona G, Ghigo D, Bosia A. Nitric oxide reverts the resistance to doxorubicin in human colon cancer cells by inhibiting the drug efflux. Cancer Res. 2005; 65:516–525.

56. Kopecka J, Salzano G, Campia I, Lusa S, Ghigo D, De Rosa G, Riganti C. Insights in the chemical components of liposomes responsible for P-glycoprotein inhibition. Nanomedicine. 2014; 10:77–87.

SUPPLEMENTARY FIGURES AND TABLES

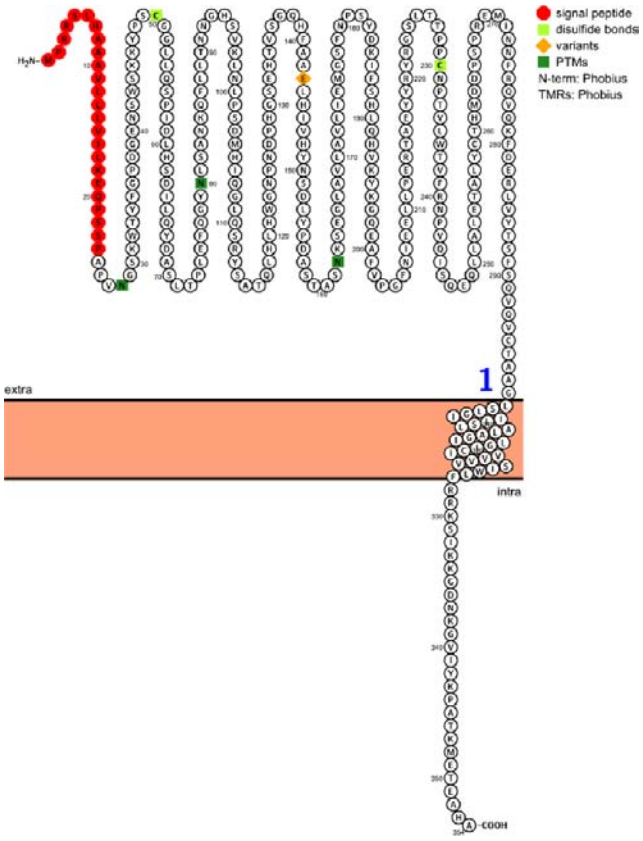

Supplementary Figure 1: CAXII topology. The topology of CAXII was obtained with Protter software (Omasits U, Ahrens CH, Müller S, Wollscheid B. Protter: interactive protein feature visualization and integration with experimental proteomic data. *Bioinformatics* 2014; **30**: 884–886; http://wlab.ethz.ch/protter).

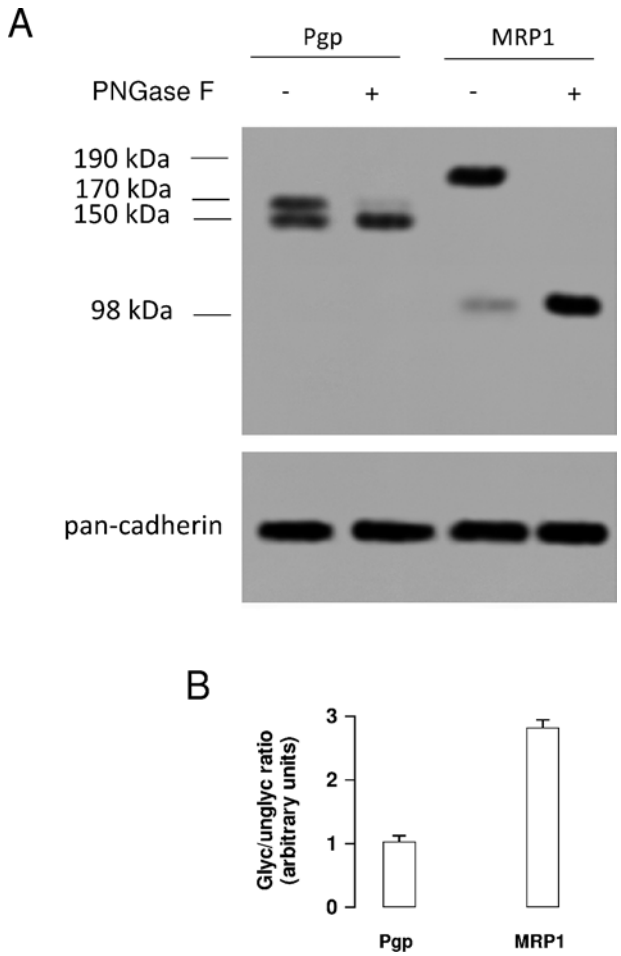

Supplementary Figure 2: Glycosylated versus deglycosylated Pgp and MRP1 in chemoresistant colon cancer cells. **(A)** Biotinylated plasma membrane extracts from human chemoresistant colon cancer HT29/dx cells were analyzed by Western blotting for the expression of Pgp and MRP1, with antibodies recognizing the glycosylated (i.e. 170 kDa band for Pgp, 190 kDa band for MRP1) and the deglycosylated (i.e. 150 kDa band for Pgp, 98 kDa band for MRP1) form of each protein. As internal control, extracts were incubated 1 h at 37°C with 1 μU of recombinant peptide-N-glycosidase F (PNGase F), to remove N-glycosylation. The pan-cadherin expression was used as a control of equal protein loading. The figure is representative of three experiments with similar results. **(B)** The densitometric analysis between glycosylated and deglycosylated bands (glyc/deglyc ratio) was performed with the ImageJ software (http://imagej.nih.gov/ij/).

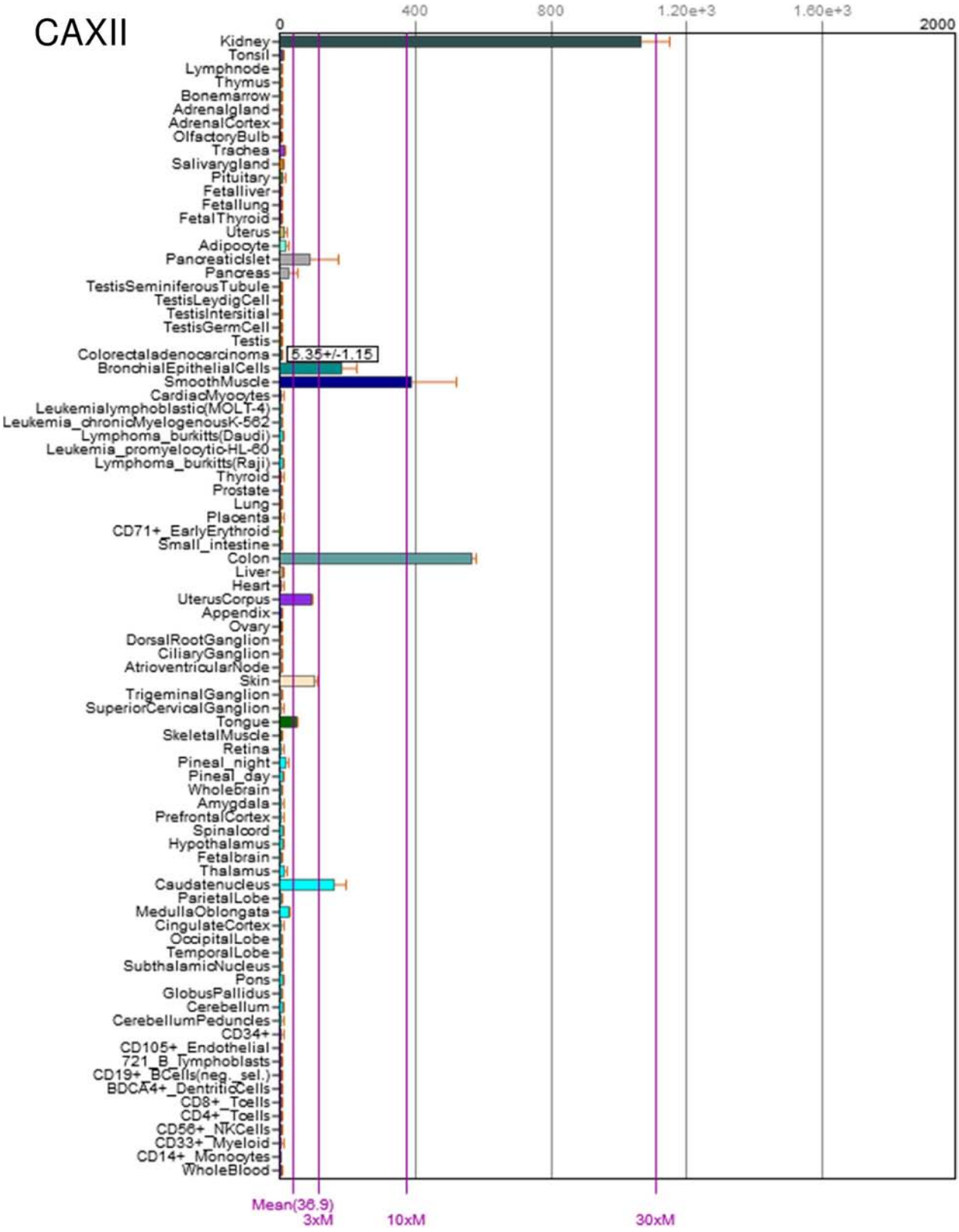

Supplementary Figure 3: Expression of CAXII in different human tissues. The expression level of CAXII was analyzed with the BioGPS tool (http://biogps.org, http://genomebiology.com/2009/10/11/R130), GeneAtlas U133A (http://www.ncbi.nlm.nih.gov/pubmed/15075390), gcrma, probe 203963_at. The relative expression level of CAXII in colon adenocarcinoma is indicated.

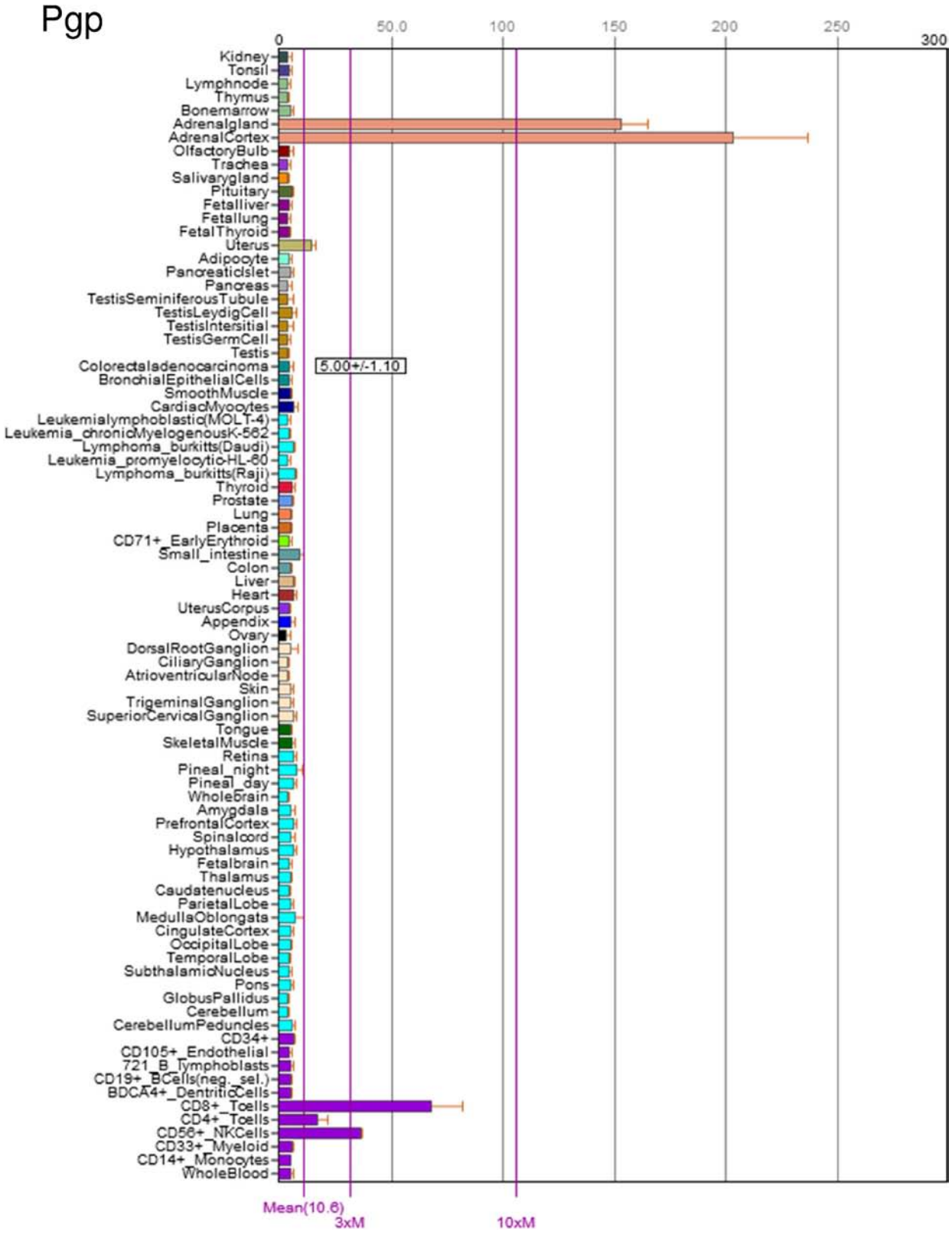

Supplementary Figure 4: Expression of Pgp in different human tissues. The expression level of Pgp was analyzed with the BioGPS tool (http://biogps.org, http://genomebiology.com/2009/10/11/R130), GeneAtlas U133A (http://www.ncbi.nlm.nih.gov/pubmed/15075390), gcrma, probe 209993_at. The relative expression level of Pgp in colon adenocarcinoma is indicated.

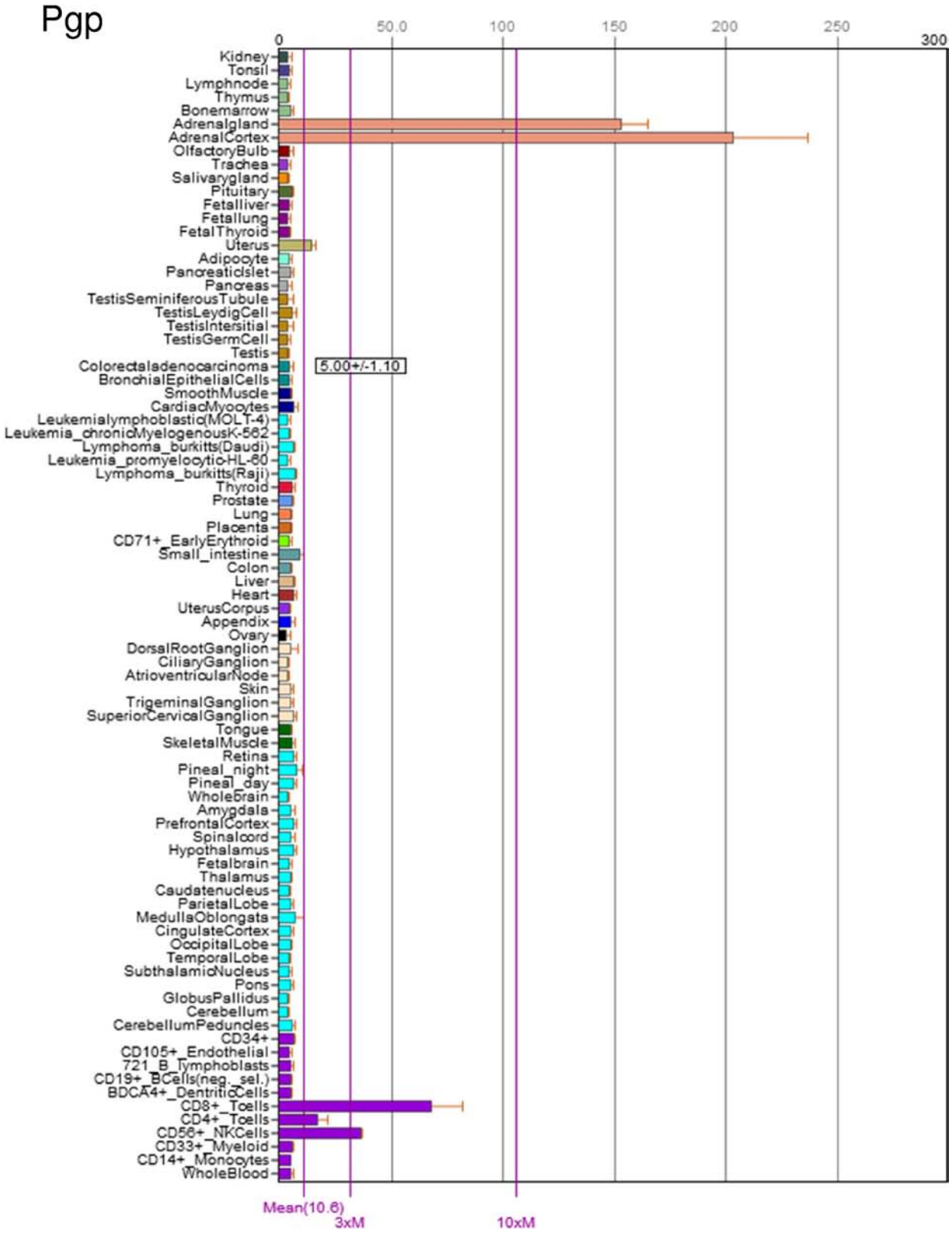

Supplementary Figure 4: Expression of Pgp in different human tissues. The expression level of Pgp was analyzed with the BioGPS tool (http://biogps.org, http://genomebiology.com/2009/10/11/R130), GeneAtlas U133A (http://www.ncbi.nlm.nih.gov/pubmed/15075390), gcrma, probe 209993_at. The relative expression level of Pgp in colon adenocarcinoma is indicated.

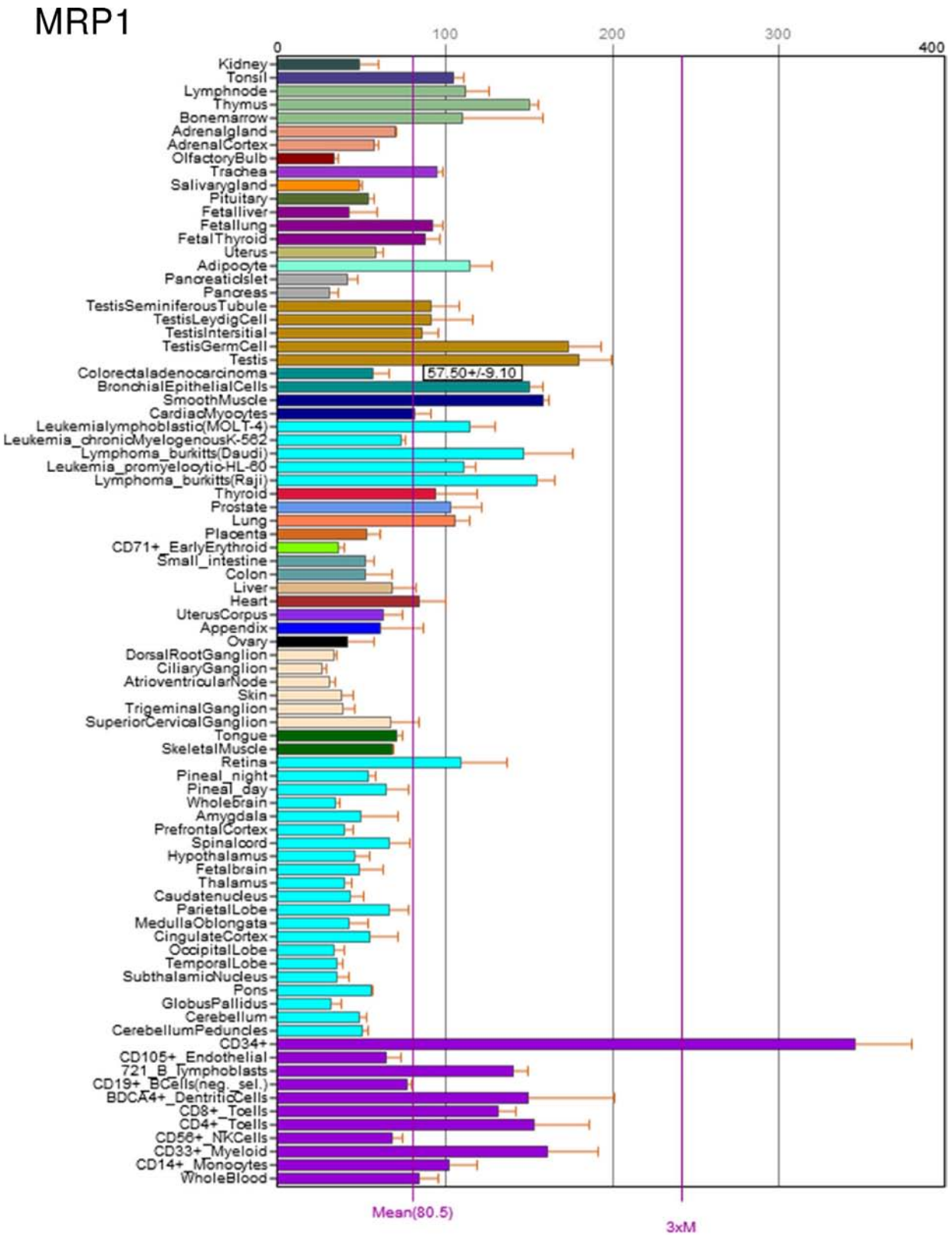

Supplementary Figure 5: Expression of MRP1 in different human tissues. The expression level of MRP1 was analyzed with the BioGPS tool (http://biogps.org, http://genomebiology.com/2009/10/11/R130), GeneAtlas U133A (http://www.ncbi.nlm.nih.gov/pubmed/15075390), gcrma, probe 202804_at. The relative expression level of MRP1 in colon adenocarcinoma is indicated.

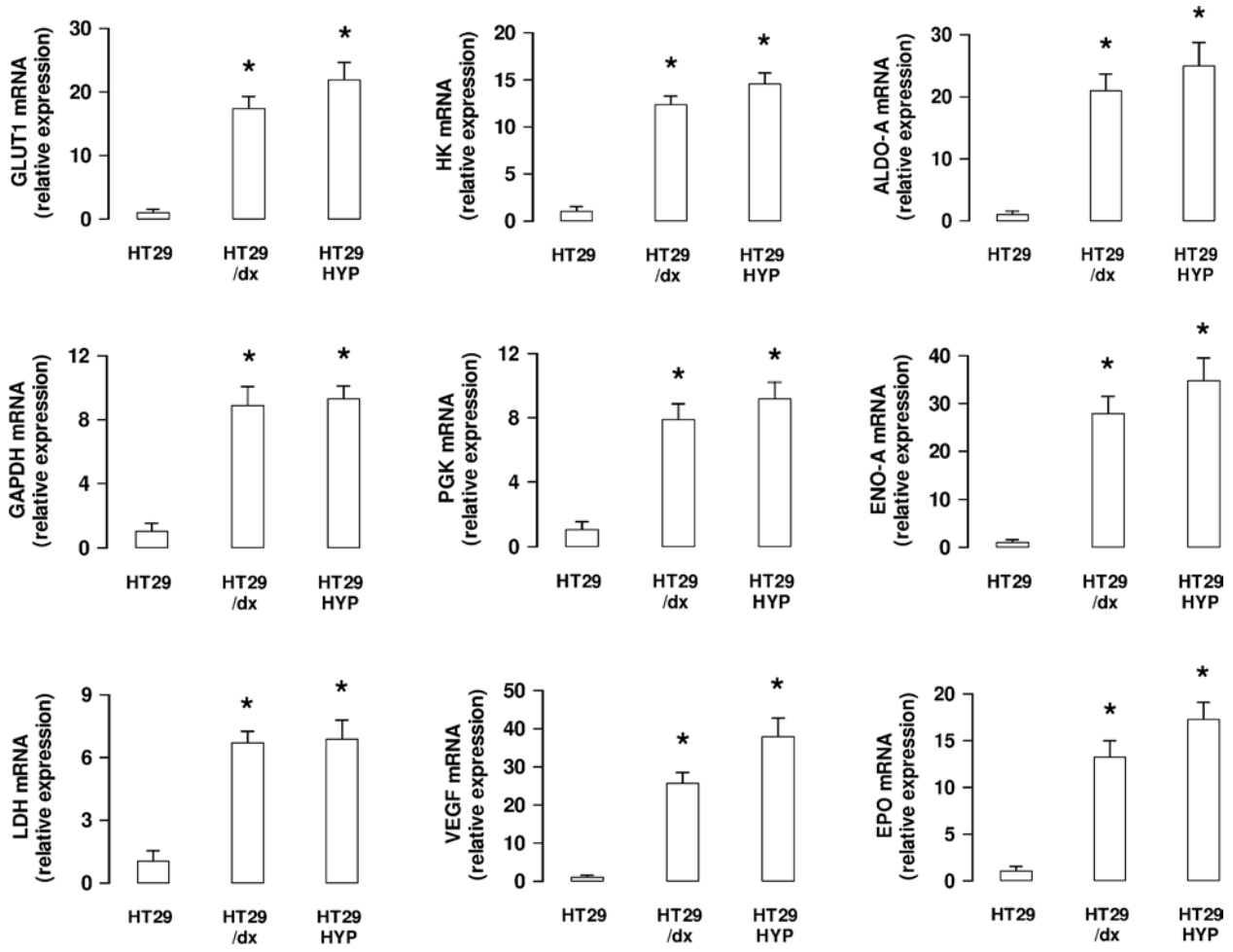

Supplementary Figure 6: Expression of HIF-1α target genes in chemosensitive and chemoresistant colon cancer cells. The mRNA level of glucose transporter 1 (*GLUT1*), hexokinase (*HK*), aldolase-A (*ALDO-A*), glyceraldehyde 3-phosphate dehydrogenase (*GAPDH*), phosphoglycerate kinase (*PGK*), enolase-A (*ENO-A*), lactate dehydrogenase (*LDH*), vascular endothelial growth factor (*VEGF*), erythropoietin (*EPO*) was detected by qRT-PCR in normoxic HT29 and HT29/dx cells. As positive control of HIF-1α activation, the expression of the same mRNAs was measured in HT29 cultured in hypoxic conditions (2% O_2 for 24 h; HYP). Data are presented as means ± SD ($n = 4$). For all panels, versus normoxic HT29: * $p < 0.001$.

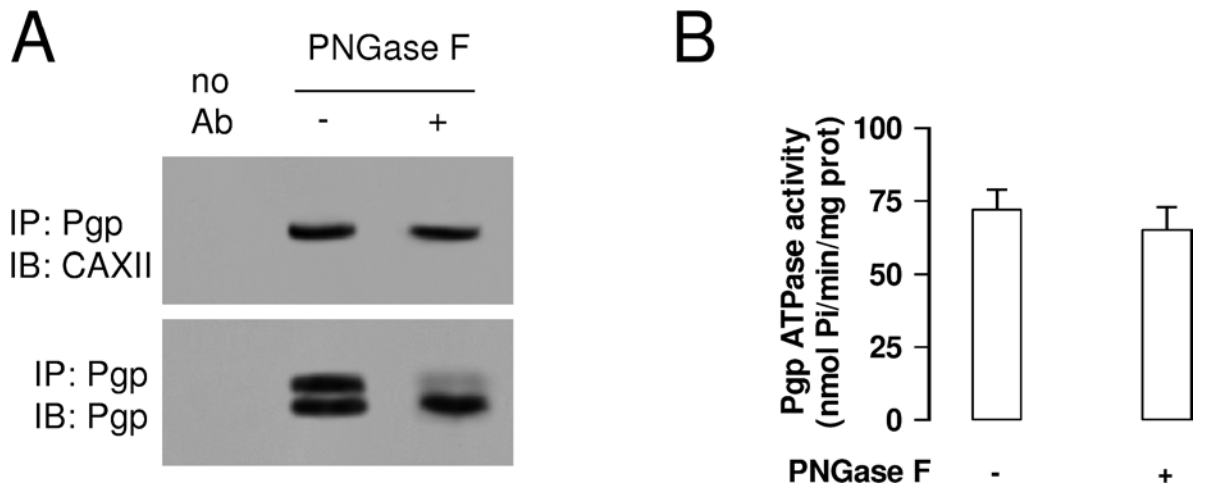

Supplementary Figure 7: CAXII is associated with both glycosylated and deglycosylated Pgp. (A) Biotinylated plasma membrane extracts from human chemoresistant colon cancer HT29/dx cells were incubated 1 h at 37°C with (+) or without (−) 1 μU of PNGase F, immunoprecipitated (IP) with an anti-Pgp antibody recognizing both the glycosylated and the deglycosylated form of Pgp, then immunoblotted (IB) with an anti-CAXII or an anti-Pgp antibody. No Ab: samples immunoprecipitated without antibody. The figure is representative of two experiments with similar results. **(B)** Pgp ATPase activity was measured spectrophotometrically on Pgp-rich vesicles extracted from membrane fractions, pre-treated or not with PNGase F as reported in A. Data are presented as means ± SD (n = 3).

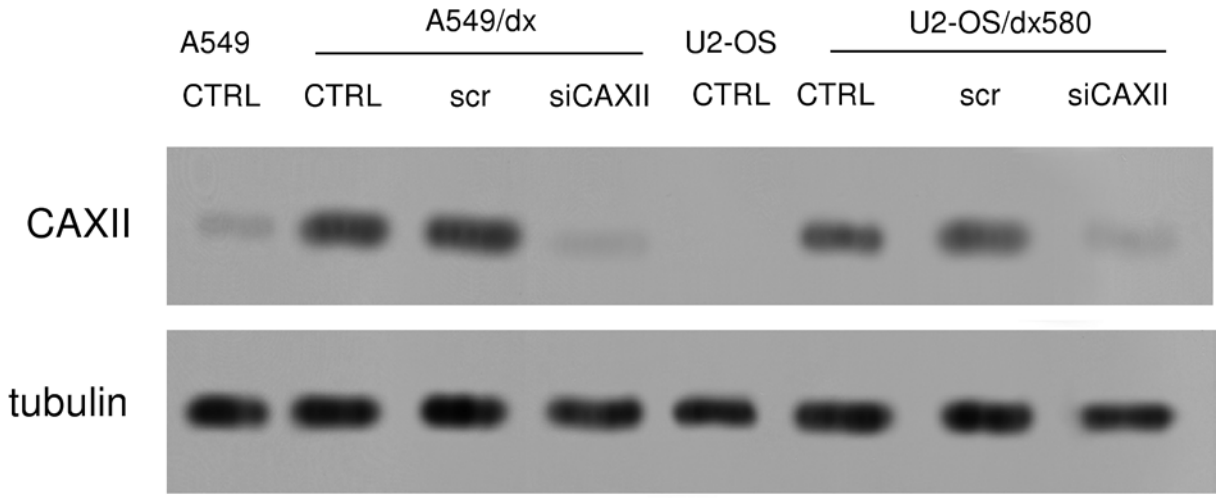

Supplementary Figure 8: CAXII silencing in lung and osteosarcoma chemoresistant cells. Human chemoresistant lung cancer A549/dx cells and osteosarcoma U2-OS/dx580 cells were cultured for 48 h with fresh medium (CTRL), treated with a non targeting scrambled siRNA (scr) or with a CAXII-targeting specific siRNA pool (siCAXII). Chemosensitive A549 and U2-OS cells were included as control. The expression of CAXII was measured in whole cell lysates by Western blotting. The β-tubulin expression was used as a control of equal protein loading. The figure is representative of two experiments with similar results.

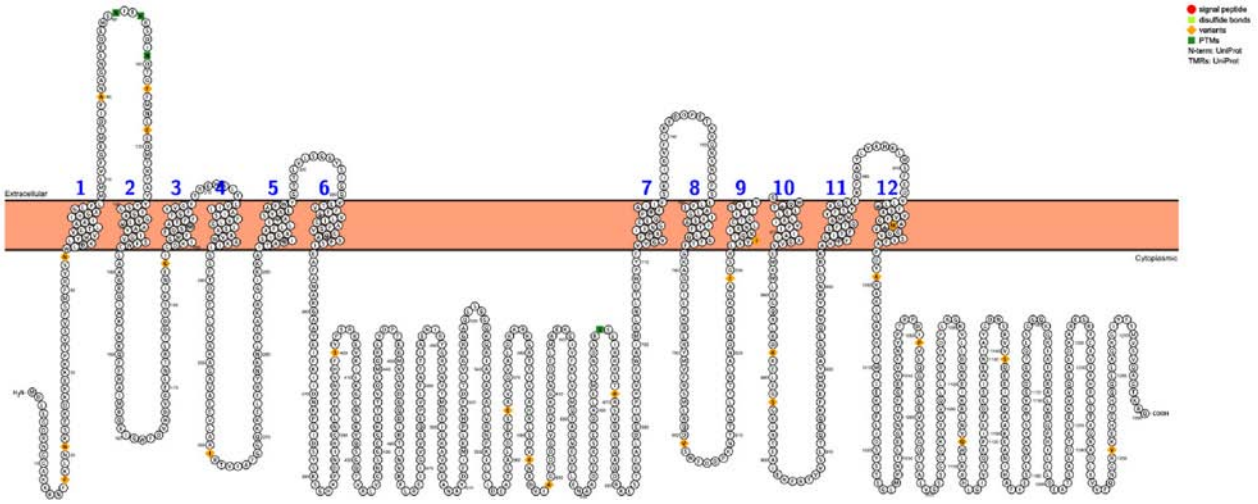

Supplementary Figure 9: Pgp topology. The topology of Pgp was obtained with Protter software (Omasits U, Ahrens CH, Müller S, Wollscheid B. Protter: interactive protein feature visualization and integration with experimental proteomic data. *Bioinformatics* 2014; **30**: 884–886; http://wlab.ethz.ch/protter).

Supplemental Table 1. Quantitative analysis of glycoproteins present on HT29 and HT29/dx cells surface

Accession	UP symbol	Gene name	CD	Peptide counted	Peptide used for quantitation	Normalized abundance HT29/dx untreated	Normalized abundance HT29 untreated	Log2 ratio DX/HT29 untretaed	Surfaceome	Phobius TM	Description
O15460	P4HA2_HUMAN	P4HA2		1	1	9.98E+00	3.33E+04	-11.704		0	Prolyl 4-hydroxylase subunit alpha-2
P08571	CD14_HUMAN	CD14	CD14	1	1	9.98E+00	2.04E+04	-10.997		GPI	Monocyte differentiation antigen CD14
Q92876	KLK6_HUMAN	KLK6		1	1	9.98E+00	1.22E+04	-10.261		0	Kallikrein-6
O95302	FKBP9_HUMAN	FKBP9		3	3	8.10E+02	1.16E+05	-7.160		0	Peptidyl-prolyl cis-trans isomerase FKBP9
Q9UNN8	EPCR_HUMAN	PROCR	CD201	2	1	2.61E+02	2.74E+04	-6.717	Y	1	Endothelial protein C receptor
O60512	B4GT3_HUMAN	B4GALT3		1	1	6.95E+02	6.59E+04	-6.566		0	Beta-1,4-galactosyltransferase 3
P30533	AMRP_HUMAN	LRPAP1		1	1	8.72E+02	7.07E+04	-6.343		0	Alpha-2-macroglobulin receptor-associated protein
P55082	MFAP3_HUMAN	MFAP3		1	1	1.04E+02	7.74E+03	-6.213		1	Microfibril-associated glycoprotein 3
P04066	FUCO_HUMAN	FUCA1		1	1	7.95E+01	2.69E+03	-5.083		0	Tissue alpha-L-fucosidase
Q5PT55	NTCP5_HUMAN	SLC10A5		1	1	9.87E+01	3.15E+03	-4.997	Y	9	Sodium\bile acid cotransporter 5
P18084	ITB5_HUMAN	ITGB5		1	1	2.38E+03	7.14E+04	-4.909	Y	1	Integrin beta-5
O60704	TPST2_HUMAN	TPST2		1	1	7.03E+02	1.87E+04	-4.731		0	Protein-tyrosine sulfotransferase 2
P30825	CTR1_HUMAN	SLC7A1		7	7	2.73E+05	6.28E+06	-4.526	Y	14	High affinity cationic amino acid transporter 1
Q9H6Y7	RN167_HUMAN	RNF167		2	2	2.58E+03	5.43E+04	-4.395	Y	1	E3 ubiquitin-protein ligase RNF167
P55268	LAMB2_HUMAN	LAMB2		1	1	2.00E+03	4.20E+04	-4.392		0	Laminin subunit beta-2
Q14435	GALT3_HUMAN	GALNT3		2	2	2.03E+03	3.52E+04	-4.118		1	Polypeptide N-acetylgalactosaminyltransferase 3
P54851	EMP2_HUMAN	EMP2		1	1	8.79E+03	1.44E+05	-4.029	Y	3	Epithelial membrane protein 2
P55058	PLTP_HUMAN	PLTP		3	3	2.99E+03	4.72E+04	-3.984		0	Phospholipid transfer protein
Q09327	MGAT3_HUMAN	MGAT3		2	2	2.96E+03	4.57E+04	-3.948		0	Beta-1,4-mannosyl-glycoprotein 4-beta-N-acetylglucosaminyltransferase
Q13443	ADAM9_HUMAN	ADAM9		2	2	5.72E+03	8.02E+04	-3.809	Y	1	Disintegrin and metalloproteinase domain-containing protein 9
O43852	CALU_HUMAN	CALU		1	1	4.11E+04	5.73E+05	-3.799		0	Calumenin
P54852	EMP3_HUMAN	EMP3		1	1	2.36E+02	3.23E+03	-3.778	Y	3	Epithelial membrane protein 3
P30443	1A01_HUMAN	HLA-A		3	3	1.11E+04	1.45E+05	-3.707	Y	1	HLA class I histocompatibility antigen, A-1 alpha chain
Q9UQV4	LAMP3_HUMAN	LAMP3	CD208	1	1	5.73E+03	7.40E+04	-3.692		1	Lysosome-associated membrane glycoprotein 3

Q10589	BST2_HUMAN	BST2	CD317	9	9	3.87E+05	4.69E+06	-3.599		1, GPI	Bone marrow stromal antigen 2
P09958	FURIN_HUMAN	FURIN		2	2	1.27E+04	1.44E+05	-3.505		1	Furin
Q9C0K1	S39A8_HUMAN	SLC39A8		2	2	9.69E+03	1.05E+05	-3.431	Y	6	Zinc transporter ZIP8
P30685	1B35_HUMAN	HLA-B		2	2	1.23E+04	1.32E+05	-3.426	Y	1	HLA class I histocompatibility antigen, B-35 alpha chain
O96005	CLPT1_HUMAN	CLPTM1		3	3	8.05E+04	8.08E+05	-3.327	Y	5	Cleft lip and palate transmembrane protein 1
P02786	TFR1_HUMAN	TFRC	CD71	1	1	3.12E+04	2.85E+05	-3.191	Y	1, GPI	Transferrin receptor protein 1
Q96T83	SL9A7_HUMAN	SLC9A7		2	2	2.48E+04	2.21E+05	-3.155		13	Sodium\hydrogen exchanger 7
P04439	1A03_HUMAN	HLA-A		1	1	2.56E+03	2.23E+04	-3.125	Y	1	HLA class I histocompatibility antigen, A-3 alpha chain
Q9Y666	S12A7_HUMAN	SLC12A7		3	3	8.78E+04	7.40E+05	-3.076	Y	12	Solute carrier family 12 member 7
Q9NRB3	CHSTC_HUMAN	CHST12		3	3	1.91E+04	1.56E+05	-3.032		1	Carbohydrate sulfotransferase 12
Q96G97	BSCL2_HUMAN	BSCL2		2	2	3.38E+04	2.61E+05	-2.949		3	Seipin
P57057	GLPT_HUMAN	SLC37A1		2	2	1.95E+04	1.49E+05	-2.936	Y	12	Glycerol-3-phosphate transporter
Q8NHS3	MFSD8_HUMAN	MFSD8		1	1	2.36E+04	1.64E+05	-2.800	Y	12	Major facilitator superfamily domain-containing protein 8
Q9UQ53	MGT4B_HUMAN	MGAT4B		1	1	1.38E+05	9.52E+05	-2.782		0	Alpha-1,3-mannosyl-glycoprotein 4-beta-N-acetylglucosaminyltransferase B
Q15758	AAAT_HUMAN	SLC1A5		8	8	2.47E+06	1.69E+07	-2.772	Y	9	Neutral amino acid transporter B(0)
Q8IZA0	K319L_HUMAN	KIAA0319L		2	2	1.37E+04	9.38E+04	-2.771	Y	2	Uncharacterized protein KIAA0319-like
Q6YBV0	S36A4_HUMAN	SLC36A4		2	2	1.37E+04	9.18E+04	-2.749	Y	10	Proton-coupled amino acid transporter 4
P09758	TACD2_HUMAN	TACSTD2		3	3	2.63E+04	1.73E+05	-2.723	Y	1	Tumor-associated calcium signal transducer 2
P11117	PPAL_HUMAN	ACP2		3	3	1.21E+04	7.90E+04	-2.700		1	Lysosomal acid phosphatase
O60449	LY75_HUMAN	LY75	CD205	4	4	1.08E+05	6.93E+05	-2.677	Y	1	Lymphocyte antigen 75
O43567	RNF13_HUMAN	RNF13		1	1	6.28E+03	4.01E+04	-2.676		1	RING finger protein 13
Q6ZRP7	QSOX2_HUMAN	QSOX2		3	2	8.43E+04	4.94E+05	-2.551	Y	1	Sulfhydryl oxidase 2
P04062	GLCM_HUMAN	GBA		6	5	1.57E+05	8.65E+05	-2.462		0	Glucosylceramidase
Q70UQ0	IKIP_HUMAN	IKIP		1	1	1.37E+03	7.49E+03	-2.455		1	Inhibitor of nuclear factor kappa-B kinase-interacting protein
Q5TF39	NAGT1_HUMAN	NAGLT1		1	1	1.20E+04	6.53E+04	-2.445		11	Sodium-dependent glucose transporter 1
P08069	IGF1R_HUMAN	IGF1R	CD221	5	5	8.17E+04	4.40E+05	-2.430	Y	1	Insulin-like growth factor 1 receptor
Q9NYU2	UGGG1_HUMAN	UGGT1		1	1	2.59E+04	1.39E+05	-2.426		1	UDP-glucose:glycoprotein glucosyltransferase 1
Q5T2D2	TRML2_HUMAN	TREML2		1	1	2.36E+03	1.22E+04	-2.368	Y	1	Trem-like transcript 2 protein
P11279	LAMP1_HUMAN	LAMP1	CD107a	26	25	1.02E+06	5.03E+06	-2.305	Y	1	Lysosome-associated membrane glycoprotein 1
Q7Z2K6	ERMP1_HUMAN	ERMP1		2	2	1.13E+04	5.43E+04	-2.267	Y	10	Endoplasmic reticulum metallopeptidase 1

P53794	SC5A3_HUMAN	SLC5A3		1	1	8.48E+03	4.08E+04	-2.265		13	Sodium\myo-inositol cotransporter
Q7Z3C6	ATG9A_HUMAN	ATG9A		1	1	2.66E+03	1.25E+04	-2.236	Y	4	Autophagy-related protein 9A
Q687X5	STEA4_HUMAN	STEAP4		1	1	2.06E+04	9.65E+04	-2.230	Y	6	Metalloreductase STEAP4
Q9Y2E5	MA2B2_HUMAN	MAN2B2		1	1	8.40E+03	3.91E+04	-2.217		0	Epididymis-specific alpha-mannosidase
Q99808	S29A1_HUMAN	SLC29A1		3	3	2.76E+05	1.28E+06	-2.211	Y	11	Equilibrative nucleoside transporter 1
Q11201	SIA4A_HUMAN	ST3GAL1		17	17	4.66E+05	2.15E+06	-2.208		0	CMP-N-acetylneuraminate-beta-galactosamide-alpha-2,3-sialyltransferase 1
Q4ZIN3	MBRL_HUMAN	C19orf6		1	1	1.12E+04	5.15E+04	-2.199	Y	6	Membralin
Q16769	QPCT_HUMAN	QPCT		1	1	1.09E+04	4.86E+04	-2.157		0	Glutaminyl-peptide cyclotransferase
P49281	NRAM2_HUMAN	SLC11A2		1	1	9.26E+04	4.12E+05	-2.154	Y	12	Natural resistance-associated macrophage protein 2
Q8NBW4	S38A9_HUMAN	SLC38A9		1	1	2.20E+03	9.70E+03	-2.139	Y	11	Putative sodium-coupled neutral amino acid transporter 9
O15438	MRP3_HUMAN	ABCC3		2	2	1.37E+04	5.73E+04	-2.065	Y	17	Canalicular multispecific organic anion transporter 2
P19526	FUT1_HUMAN	FUT1		1	1	5.40E+04	2.22E+05	-2.040		0	Galactoside 2-alpha-L-fucosyltransferase 1
Q9NV96	CC50A_HUMAN	TMEM30A		2	2	6.49E+04	2.65E+05	-2.031	Y	2	Cell cycle control protein 50A
Q8NCR9	CLRN3_HUMAN	CLRN3		1	1	3.12E+04	1.27E+05	-2.027	Y	4	Clarin-3
Q9NXG6	P4HTM_HUMAN	P4HTM		1	1	9.17E+03	3.70E+04	-2.014		1	Transmembrane prolyl 4-hydroxylase
Q9H330	CI005_HUMAN	C9orf5		2	2	1.71E+04	6.90E+04	-2.012	Y	16	Transmembrane protein C9orf5
O75063	FA20B_HUMAN	FAM20B		2	2	7.95E+03	3.19E+04	-2.004		0	Protein FAM20B
P30450	1A26_HUMAN	HLA-A		1	1	9.26E+04	3.70E+05	-1.998	Y	1	HLA class I histocompatibility antigen, A-26 alpha chain
Q9UIQ6	LCAP_HUMAN	LNPEP		7	7	3.24E+05	1.25E+06	-1.948	Y	1	Leucyl-cystinyl aminopeptidase
Q96AY3	FKB10_HUMAN	FKBP10		3	3	1.25E+04	4.77E+04	-1.929		0	Peptidyl-prolyl cis-trans isomerase FKBP10
Q9NQ84	GPC5C_HUMAN	GPRC5C		1	1	2.81E+04	1.06E+05	-1.920	Y	7	G-protein coupled receptor family C group 5 member C
A1A5B4	ANO9_HUMAN	ANO9		2	2	2.60E+04	9.67E+04	-1.895	Y	8	Anoctamin-9
Q0P6H9	TMM62_HUMAN	TMEM62		2	2	1.47E+04	5.46E+04	-1.893	Y	5	Transmembrane protein 62
Q9NX62	IMPA3_HUMAN	IMPAD1		3	3	2.26E+05	8.17E+05	-1.856		1	Inositol monophosphatase 3
Q8IV08	PLD3_HUMAN	PLD3		2	2	2.10E+05	7.44E+05	-1.826	Y	1	Phospholipase D3
O94923	GLCE_HUMAN	GLCE		1	1	7.46E+03	2.62E+04	-1.811		0	D-glucuronyl C5-epimerase
Q12913	PTPRJ_HUMAN	PTPRJ	CD148	6	5	1.06E+05	3.69E+05	-1.803	Y	1	Receptor-type tyrosine-protein phosphatase eta
P56199	ITA1_HUMAN	ITGA1	CD49a	8	8	2.86E+05	9.97E+05	-1.801		1	Integrin alpha-1
P07339	CATD_HUMAN	CTSD		2	2	1.25E+05	4.30E+05	-1.776		0	Cathepsin D
Q3ZCQ3	F174B_HUMAN	FAM174B		1	1	3.76E+05	1.28E+06	-1.766	Y	1	Membrane protein FAM174B

Q9BXS4	TMM59_HUMAN	TMEM59		3	3	8.28E+04	2.76E+05	-1.739	Y	1	Transmembrane protein 59
O00469	PLOD2_HUMAN	PLOD2		2	2	8.39E+03	2.79E+04	-1.735		0	Procollagen-lysine,2-oxoglutarate 5-dioxygenase 2
Q5XXA6	ANO1_HUMAN	ANO1		2	2	7.09E+03	2.24E+04	-1.663	Y	8	Anoctamin-1
Q7LGA3	HS2ST_HUMAN	HS2ST1		2	2	9.15E+04	2.87E+05	-1.650		0	Heparan sulfate 2-O-sulfotransferase 1
Q9C0H2	TTYH3_HUMAN	TTYH3		2	2	6.84E+04	2.14E+05	-1.644	Y	5	Protein tweety homolog 3
Q8N0Z9	YL020_HUMAN			3	3	2.62E+04	8.17E+04	-1.642		1	Ig-like domain-containing protein FLJ20674 SV=1
Q12767	K0195_HUMAN	KIAA0195		1	1	8.88E+03	2.69E+04	-1.598	Y	10	Uncharacterized protein KIAA0195
Q9HBB8	MUCDL_HUMAN	MUPCDH		4	4	1.51E+05	4.55E+05	-1.594	Y	1	Mucin and cadherin-like protein
P02749	APOH_HUMAN	APOH		1	1	5.48E+03	1.64E+04	-1.582		0	Beta-2-glycoprotein 1
Q8NBN3	TM87A_HUMAN	TMEM87A		9	8	4.57E+06	1.36E+07	-1.570	Y	7	Transmembrane protein 87A
Q9H2A7	CXL16_HUMAN	CXCL16		1	1	7.13E+02	2.11E+03	-1.566	Y	1	C-X-C motif chemokine 16
P13688	CEAM1_HUMAN	CEACAM1	CD66a	3	3	1.09E+05	3.20E+05	-1.554	Y	1	Carcinoembryonic antigen-related cell adhesion molecule 1
Q9NXL6	SIDT1_HUMAN	SIDT1		1	1	8.44E+03	2.45E+04	-1.540	Y	11	SID1 transmembrane family member 1
P07858	CATB_HUMAN	CTSB		1	1	4.52E+04	1.31E+05	-1.530		0	Cathepsin B
P00533	EGFR_HUMAN	EGFR		2	2	1.46E+05	4.18E+05	-1.513	Y	1	Epidermal growth factor receptor
P80188	NGAL_HUMAN	LCN2		1	1	7.82E+04	2.21E+05	-1.498		0	Neutrophil gelatinase-associated lipocalin
O00461	GOLI4_HUMAN	GOLIM4		2	2	6.74E+04	1.90E+05	-1.497		1	Golgi integral membrane protein 4
Q96BQ1	FAM3D_HUMAN	FAM3D		2	2	5.00E+04	1.41E+05	-1.494		1	Protein FAM3D
Q96NT5	PCFT_HUMAN	SLC46A1		1	1	3.53E+04	9.85E+04	-1.480	Y	11	Proton-coupled folate transporter
O75071	K0494_HUMAN	KIAA0494		3	3	2.73E+05	7.48E+05	-1.453		1	EF-hand domain-containing protein KIAA0494
O43291	SPIT2_HUMAN	SPINT2		3	3	1.50E+05	4.09E+05	-1.450	Y	1	Kunitz-type protease inhibitor 2
O15321	TM9S1_HUMAN	TM9SF1		1	1	6.29E+04	1.68E+05	-1.419	Y	9	Transmembrane 9 superfamily member 1
O00468	AGRIN_HUMAN	AGRN		5	4	1.69E+05	4.50E+05	-1.419		0	Agrin
Q9Y5Y6	ST14_HUMAN	ST14		4	4	2.46E+05	6.33E+05	-1.366	Y	1	Suppressor of tumorigenicity 14 protein
Q9Y639	NPTN_HUMAN	NPTN		7	7	5.05E+04	1.27E+05	-1.335	Y	1	Neuroplastin
Q6EMK4	VASN_HUMAN	VASN		1	1	9.59E+02	2.42E+03	-1.334	Y	1	Vasorin
Q14108	SCRB2_HUMAN	SCARB2		18	17	7.53E+06	1.89E+07	-1.330	Y	1	Lysosome membrane protein 2
Q8N697	S15A4_HUMAN	SLC15A4		3	3	1.70E+05	4.28E+05	-1.326	Y	13	Solute carrier family 15 member 4
Q99523	SORT_HUMAN	SORT1		3	3	1.83E+05	4.59E+05	-1.325		1	Sortilin
Q93050	VPP1_HUMAN	ATP6V0A1		1	1	7.08E+04	1.76E+05	-1.310	Y	8	V-type proton ATPase 116 kDa subunit a isoform 1

Q8NBJ4	GOLM1_HUMAN	GOLM1		2	2	1.51E+06	3.72E+06	-1.305		0	Golgi membrane protein 1
Q9HAS3	S28A3_HUMAN	SLC28A3		1	1	1.13E+04	2.78E+04	-1.302	Y	13	Solute carrier family 28 member 3
Q9NZP8	C1RL_HUMAN	C1RL		1	1	8.26E+03	2.02E+04	-1.291		0	Complement C1r subcomponent-like protein
P21589	5NTD_HUMAN	NT5E	CD73	3	3	2.32E+05	5.53E+05	-1.253	Y	1, GPI	5'-nucleotidase
Q6P4E1	CASC4_HUMAN	CASC4		4	4	3.18E+04	7.54E+04	-1.247		1	Protein CASC4
Q9NUN5	LMBD1_HUMAN	LMBRD1		9	9	7.56E+05	1.78E+06	-1.237	Y	9	Probable lysosomal cobalamin transporter
P49641	MA2A2_HUMAN	MAN2A2		2	2	2.18E+04	5.08E+04	-1.218		1	Alpha-mannosidase 2x
Q11206	SIA4C_HUMAN	ST3GAL4		8	8	5.37E+05	1.24E+06	-1.211		0	CMP-N-acetylneuraminate-beta-galactosamide-alpha-2,3-sialyltransferase 4
Q08380	LG3BP_HUMAN	LGALS3BP		17	17	1.49E+07	3.44E+07	-1.211		0	Galectin-3-binding protein
P42892	ECE1_HUMAN	ECE1		19	19	6.51E+05	1.50E+06	-1.200	Y	1	Endothelin-converting enzyme 1
Q13586	STIM1_HUMAN	STIM1		4	4	2.92E+05	6.64E+05	-1.184	Y	1	Stromal interaction molecule 1
Q16563	SYPL1_HUMAN	SYPL1		2	2	8.80E+04	1.99E+05	-1.180	Y	3	Synaptophysin-like protein 1
Q04900	MUC24_HUMAN	CD164	CD164	2	2	2.25E+04	5.08E+04	-1.176	Y	0	Sialomucin core protein 24
P43307	SSRA_HUMAN	SSR1		3	3	2.54E+04	5.72E+04	-1.171		1	Translocon-associated protein subunit alpha
Q7Z6M3	MCA32_HUMAN	MCA32		1	1	1.65E+04	3.68E+04	-1.160		1	Probable mast cell antigen 32 homolog
Q8TEM1	PO210_HUMAN	NUP210		5	5	2.36E+05	5.25E+05	-1.151		1	Nuclear pore membrane glycoprotein 210
Q4KMQ2	ANO6_HUMAN	ANO6		3	3	9.77E+04	2.15E+05	-1.135	Y	8	Anoctamin-6
P14625	ENPL_HUMAN	HSP90B1		5	5	9.77E+05	2.12E+06	-1.121		0	Endoplasmin
Q13510	ASAH1_HUMAN	ASAH1		1	1	1.04E+04	2.25E+04	-1.119		0	Acid ceramidase
Q8WWB7	NCUG1_HUMAN	C1orf85		5	5	2.50E+05	5.34E+05	-1.095	Y	1	Lysosomal protein NCU-G1
Q7Z4H8	KDEL2_HUMAN	KDELC2		3	3	4.44E+04	9.47E+04	-1.092		0	KDEL motif-containing protein 2
Q68CQ7	GL8D1_HUMAN	GLT8D1		3	3	1.27E+05	2.67E+05	-1.070		0	Glycosyltransferase 8 domain-containing protein 1
Q06481	APLP2_HUMAN	APLP2		2	2	1.01E+05	2.13E+05	-1.070		1	Amyloid-like protein 2
Q86YB8	ERO1B_HUMAN	ERO1LB		1	1	9.23E+04	1.92E+05	-1.055		0	ERO1-like protein beta
Q8NBK3	SUMF1_HUMAN	SUMF1		1	1	2.38E+04	4.92E+04	-1.048		0	Sulfatase-modifying factor 1
Q969N2	PIGT_HUMAN	PIGT		1	1	9.22E+03	1.89E+04	-1.038		1	GPI transamidase component PIG-T
Q8N6G5	CGAT2_HUMAN	CSGALNACT2		1	1	1.40E+04	2.87E+04	-1.031		1	Chondroitin sulfate N-acetylgalactosaminyltransferase 2
O00299	CLIC1_HUMAN	CLIC1		1	1	1.75E+04	3.55E+04	-1.025		0	Chloride intracellular channel protein 1
Q96G23	LASS2_HUMAN	LASS2		2	2	5.19E+04	1.06E+05	-1.023		6	LAG1 longevity assurance homolog 2
Q9Y653	GPR56_HUMAN	GPR56		4	3	6.65E+04	1.34E+05	-1.009	Y	7	G-protein coupled receptor 56

O95477	ABCA1_HUMAN	ABCA1	4	4	3.48E+04	6.70E+04	-0.943	Y	14	ATP-binding cassette sub-family A member 1
O15230	LAMA5_HUMAN	LAMA5	3	3	7.36E+04	1.40E+05	-0.931		0	Laminin subunit alpha-5
Q9NPC4	A4GAT_HUMAN	A4GALT	2	2	1.36E+05	2.59E+05	-0.928		1	Lactosylceramide 4-alpha-galactosyltransferase
Q16706	MA2A1_HUMAN	MAN2A1	2	2	6.16E+05	1.17E+06	-0.922		1	Alpha-mannosidase 2
O75976	CBPD_HUMAN	CPD	16	15	2.41E+06	4.49E+06	-0.895	Y	1, GPI	Carboxypeptidase D
O95857	TSN13_HUMAN	TSPAN13	6	6	3.11E+05	5.72E+05	-0.879	Y	4	Tetraspanin-13
Q9BZM5	N2DL2_HUMAN	ULBP2	4	4	3.96E+04	7.27E+04	-0.876	Y	1, GPI	NKG2D ligand 2
Q9NYU1	UGGG2_HUMAN	UGGT2	1	1	3.02E+03	5.55E+03	-0.875		0	UDP-glucose:glycoprotein glucosyltransferase 2
Q96J42	TXD15_HUMAN	TXNDC15	3	2	7.18E+04	1.31E+05	-0.870	Y	1	Thioredoxin domain-containing protein 15
Q3T906	GNPTA_HUMAN	GNPTAB	8	8	4.87E+05	8.85E+05	-0.863		2	N-acetylglucosamine-1-phosphotransferase subunits alpha\beta
O95395	GCNT3_HUMAN	GCNT3	4	3	9.01E+04	1.62E+05	-0.850		1	Beta-1,3-galactosyl-O-glycosyl-glycoprotein beta-1,6-N-acetylglucosaminyltransferase 3
P05026	AT1B1_HUMAN	ATP1B1	14	14	3.74E+06	6.74E+06	-0.848	Y	1	Sodium\potassium-transporting ATPase subunit beta-1
Q08431	MFGM_HUMAN	MFGE8	4	4	1.13E+05	2.03E+05	-0.844		0	Lactadherin
Q9H813	TM206_HUMAN	TMEM206	1	1	8.26E+04	1.46E+05	-0.827	Y	2	Transmembrane protein 206
Q5VW38	GP107_HUMAN	GPR107	6	6	2.72E+06	4.82E+06	-0.825	Y	7	Protein GPR107
Q9NXH8	CI167_HUMAN	C9orf167	1	1	8.35E+04	1.48E+05	-0.824		1	Torsin family protein C9orf167
Q9NQZ7	ENTP7_HUMAN	ENTPD7	1	1	5.32E+04	9.39E+04	-0.819	Y	2	Ectonucleoside triphosphate diphosphohydrolase 7
Q9NRX5	SERC1_HUMAN	SERINC1	3	3	1.13E+06	1.97E+06	-0.799	Y	10	Serine incorporator 1
Q8NBJ5	GT251_HUMAN	GLT25D1	4	4	4.13E+04	7.18E+04	-0.797		0	Procollagen galactosyltransferase 1
Q92673	SORL_HUMAN	SORL1	7	7	1.59E+05	2.76E+05	-0.794	Y	1	Sortilin-related receptor
Q9BZC7	ABCA2_HUMAN	ABCA2	1	1	4.45E+04	7.70E+04	-0.792	Y	14	ATP-binding cassette sub-family A member 2
P20645	MPRD_HUMAN	M6PR	6	6	1.13E+06	1.95E+06	-0.791	Y	1	Cation-dependent mannose-6-phosphate receptor
P43007	SATT_HUMAN	SLC1A4	1	1	1.65E+04	2.85E+04	-0.790	Y	9	Neutral amino acid transporter A
Q6NSJ0	K1161_HUMAN	KIAA1161	3	3	2.62E+04	4.52E+04	-0.784	Y	1	Uncharacterized family 31 glucosidase KIAA1161
Q9BXP2	S12A9_HUMAN	SLC12A9	3	3	4.93E+04	8.43E+04	-0.773	Y	13	Solute carrier family 12 member 9
P04844	RPN2_HUMAN	RPN2	2	2	4.26E+04	7.19E+04	-0.754	Y	3	Dolichyl-diphosphooligosaccharide--protein glycosyltransferase subunit 2
P10253	LYAG_HUMAN	GAA	3	3	2.35E+05	3.87E+05	-0.719		1	Lysosomal alpha-glucosidase
Q9NY97	B3GN2_HUMAN	B3GNT2	6	6	7.51E+05	1.23E+06	-0.711		1	UDP-GlcNAc:betaGal beta-1,3-N-acetylglucosaminyltransferase 2
P30989	NTR1_HUMAN	NTSR1	5	5	9.55E+05	1.55E+06	-0.697	Y	7,GPI	Neurotensin receptor type 1
Q12907	LMAN2_HUMAN	LMAN2	4	4	3.63E+05	5.84E+05	-0.688		1	Vesicular integral-membrane protein VIP36

P50895	BCAM_HUMAN	BCAM	CD239	1	1	1.91E+05	3.07E+05	-0.684		1	Basal cell adhesion molecule
Q8IWA5	CTL2_HUMAN	SLC44A2		6	5	1.64E+06	2.62E+06	-0.677	Y	10	Choline transporter-like protein 2
Q5ZPR3	CD276_HUMAN	CD276	CD276	4	4	3.24E+05	5.17E+05	-0.673	Y	1	CD276 antigen
P48029	SC6A8_HUMAN	SLC6A8		1	1	7.39E+04	1.18E+05	-0.671	Y	12	Sodium- and chloride-dependent creatine transporter 1
P78536	ADA17_HUMAN	ADAM17	CD156b	2	2	1.95E+04	3.09E+04	-0.666	Y	1	Disintegrin and metalloproteinase domain-containing protein 17
P35613	BASI_HUMAN	BSG	CD147	7	7	1.35E+06	2.14E+06	-0.662	Y	1	Basigin
P10586	PTPRF_HUMAN	PTPRF		5	4	1.38E+05	2.18E+05	-0.660	Y	1	Receptor-type tyrosine-protein phosphatase F
P07686	HEXB_HUMAN	HEXB		2	2	1.07E+05	1.68E+05	-0.657		0	Beta-hexosaminidase subunit beta
P17301	ITA2_HUMAN	ITGA2	CD49b	13	13	9.08E+05	1.43E+06	-0.654	Y	1	Integrin alpha-2
Q6P179	ERAP2_HUMAN	ERAP2		3	3	1.65E+05	2.59E+05	-0.645		0	Endoplasmic reticulum aminopeptidase 2
Q9UHW9	S12A6_HUMAN	SLC12A6		2	2	1.07E+03	1.62E+03	-0.597	Y	14	Solute carrier family 12 member 6
Q8TCJ2	STT3B_HUMAN	STT3B		14	14	6.99E+05	1.05E+06	-0.588	Y	13	Dolichyl-diphosphooligosaccharide--protein glycosyltransferase subunit STT3B
P98160	PGBM_HUMAN	HSPG2		2	2	1.33E+05	1.98E+05	-0.580		0	Basement membrane-specific heparan sulfate proteoglycan core protein
O14657	TOR1B_HUMAN	TOR1B		2	1	2.08E+03	3.07E+03	-0.559		0	Torsin-1B
Q99538	LGMN_HUMAN	LGMN		1	1	1.63E+04	2.40E+04	-0.559		0	Legumain
Q93008	USP9X_HUMAN	USP9X		1	1	3.70E+04	5.43E+04	-0.555		0	Probable ubiquitin carboxyl-terminal hydrolase FAF-X
Q96KA5	CLP1L_HUMAN	CLPTM1L		2	2	6.59E+04	9.66E+04	-0.552	Y	6	Cleft lip and palate transmembrane protein 1-like protein
Q96HA4	CA159_HUMAN	C1orf159		1	1	2.20E+04	3.19E+04	-0.540		1	Uncharacterized protein C1orf159
P54709	AT1B3_HUMAN	ATP1B3	CD298	5	5	1.54E+06	2.24E+06	-0.539	Y	1	Sodium\potassium-transporting ATPase subunit beta-3
Q16880	CGT_HUMAN	UGT8		2	2	1.09E+05	1.57E+05	-0.519		1	2-hydroxyacylsphingosine 1-beta-galactosyltransferase
P11047	LAMC1_HUMAN	LAMC1		2	2	4.27E+04	6.11E+04	-0.517		0	Laminin subunit gamma-1
Q9Y2A9	B3GN3_HUMAN	B3GNT3		1	1	4.70E+03	6.62E+03	-0.496		0	UDP-GlcNAc:betaGal beta-1,3-N-acetylglucosaminyltransferase 3
P41440	S19A1_HUMAN	SLC19A1		1	1	7.32E+04	1.03E+05	-0.496	Y	11	Folate transporter 1
O75509	TNR21_HUMAN	TNFRSF21		2	2	1.16E+05	1.63E+05	-0.492	Y	1	Tumor necrosis factor receptor superfamily member 21
Q92542	NICA_HUMAN	NCSTN		2	2	3.06E+04	4.30E+04	-0.492	Y	1	Nicastrin
P05556	ITB1_HUMAN	ITGB1	CD29	3	3	1.97E+05	2.69E+05	-0.447	Y	1	Integrin beta-1
P98172	EFNB1_HUMAN	EFNB1		3	2	5.82E+04	7.93E+04	-0.446	Y	1	Ephrin-B1
P02790	HEMO_HUMAN	HPX		1	1	3.35E+04	4.56E+04	-0.445		0	Hemopexin
Q96HE7	ERO1A_HUMAN	ERO1L		2	2	7.17E+04	9.73E+04	-0.441		0	ERO1-like protein alpha
P08962	CD63_HUMAN	CD63	CD63	2	2	9.60E+04	1.30E+05	-0.438	Y	4	CD63 antigen

P04843	RPN1_HUMAN	RPN1		2	2	2.59E+04	3.51E+04	-0.435		1	Dolichyl-diphosphooligosaccharide--protein glycosyltransferase subunit 1
Q96AQ6	PBIP1_HUMAN	PBXIP1		1	1	3.42E+04	4.62E+04	-0.432		1	Pre-B-cell leukemia transcription factor-interacting protein 1
P11717	MPRI_HUMAN	IGF2R	CD222	7	6	4.81E+05	6.45E+05	-0.422	Y	1	Cation-independent mannose-6-phosphate receptor
Q8TBP5	F174A_HUMAN	FAM174A		2	2	5.42E+05	7.24E+05	-0.416	Y	1	Membrane protein FAM174A
Q9BZR6	RTN4R_HUMAN	RTN4R		1	1	8.45E+03	1.11E+04	-0.398		GPI	Reticulon-4 receptor
Q14517	FAT1_HUMAN	FAT1		9	9	1.50E+06	1.97E+06	-0.390		1	Protocadherin Fat 1
Q9UH99	UN84B_HUMAN	UNC84B		1	1	2.02E+05	2.63E+05	-0.384		3	Protein unc-84 homolog B
Q9BU23	LMF2_HUMAN	LMF2		2	2	1.78E+04	2.32E+04	-0.383	Y	11	Lipase maturation factor 2
Q9UHG3	PCYOX_HUMAN	PCYOX1		3	3	4.10E+04	5.25E+04	-0.356		0	Prenylcysteine oxidase 1
P46977	STT3A_HUMAN	STT3A		9	8	7.35E+05	9.35E+05	-0.347	Y	13	Dolichyl-diphosphooligosaccharide--protein glycosyltransferase subunit STT3A
P15151	PVR_HUMAN	PVR	CD155	3	3	9.61E+04	1.21E+05	-0.332	Y	1	Poliovirus receptor
P30447	1A23_HUMAN	HLA-A		3	3	6.00E+04	7.41E+04	-0.306	Y	1	HLA class I histocompatibility antigen, A-23 alpha chain
Q8NE01	CNNM3_HUMAN	CNNM3		1	1	6.96E+03	8.51E+03	-0.290		3	Metal transporter CNNM3
Q86SQ4	GP126_HUMAN	GPR126		7	7	2.66E+05	3.22E+05	-0.273	Y	7	G-protein coupled receptor 126
Q9H2H9	S38A1_HUMAN	SLC38A1		1	1	1.92E+06	2.30E+06	-0.260	Y	11	Sodium-coupled neutral amino acid transporter 1
Q9UIW2	PLXA1_HUMAN	PLXNA1		1	1	4.95E+04	5.89E+04	-0.252	Y	1	Plexin-A1
P54760	EPHB4_HUMAN	EPHB4		5	5	2.80E+05	3.33E+05	-0.251	Y	1	Ephrin type-B receptor 4
Q6P4Q7	CNNM4_HUMAN	CNNM4		3	3	1.72E+05	2.03E+05	-0.239	Y	4	Metal transporter CNNM4
Q9NY35	CLDN1_HUMAN	CLDND1		2	2	2.21E+04	2.59E+04	-0.229	Y	3	Claudin domain-containing protein 1
Q86SR1	GLT10_HUMAN	GALNT10		1	1	1.05E+04	1.22E+04	-0.214		0	Polypeptide N-acetylgalactosaminyltransferase 10
P04156	PRIO_HUMAN	PRNP	CD230	1	1	1.13E+06	1.31E+06	-0.212	Y	2,GPI	Major prion protein
Q9P2C4	TM181_HUMAN	TMEM181		6	6	4.68E+05	5.38E+05	-0.201		8	Transmembrane protein 181
P22607	FGFR3_HUMAN	FGFR3	CD333	1	1	1.14E+04	1.29E+04	-0.182	Y	1	Fibroblast growth factor receptor 3
O95297	MPZL1_HUMAN	MPZL1		1	1	4.65E+05	5.27E+05	-0.180	Y	1	Myelin protein zero-like protein 1
P43251	BTD_HUMAN	BTD		2	2	1.04E+05	1.18E+05	-0.178		0	Biotinidase
Q8N766	K0090_HUMAN	KIAA0090		1	1	2.50E+05	2.83E+05	-0.174		1	Uncharacterized protein KIAA0090
P48723	HSP13_HUMAN	HSPA13		1	1	3.92E+04	4.40E+04	-0.164		0	Heat shock 70 kDa protein 13
Q15223	PVRL1_HUMAN	PVRL1	CD111	4	4	3.46E+05	3.87E+05	-0.162	Y	1	Poliovirus receptor-related protein 1
P15586	GNS_HUMAN	GNS		2	1	1.91E+04	2.13E+04	-0.158		0	N-acetylglucosamine-6-sulfatase
Q9H015	S22A4_HUMAN	SLC22A4		2	2	6.06E+04	6.75E+04	-0.156	Y	12	Solute carrier family 22 member 4

O60568	PLOD3_HUMAN	PLOD3		3	3	1.30E+05	1.43E+05	-0.137		0	Procollagen-lysine,2-oxoglutarate 5-dioxygenase 3
P08195	4F2_HUMAN	SLC3A2	CD98	21	21	2.15E+07	2.34E+07	-0.124	Y	1	4F2 cell-surface antigen heavy chain
O15533	TPSN_HUMAN	TAPBP		1	1	1.97E+04	2.14E+04	-0.120		1	Tapasin
P08581	MET_HUMAN	MET		3	3	3.42E+05	3.68E+05	-0.103	Y	1	Hepatocyte growth factor receptor
Q9NPR2	SEM4B_HUMAN	SEMA4B		6	6	4.39E+05	4.70E+05	-0.100	Y	1	Semaphorin-4B
Q96AE7	TTC17_HUMAN	TTC17		1	1	1.40E+04	1.48E+04	-0.084		0	Tetratricopeptide repeat protein 17
Q15904	VAS1_HUMAN	ATP6AP1		8	8	4.57E+05	4.85E+05	-0.083	Y	1	V-type proton ATPase subunit S1
P29317	EPHA2_HUMAN	EPHA2		5	5	1.96E+06	2.07E+06	-0.079	Y	1	Ephrin type-A receptor 2
Q12891	HYAL2_HUMAN	HYAL2		1	1	2.18E+04	2.30E+04	-0.079		GPI	Hyaluronidase-2
Q96S52	PIGS_HUMAN	PIGS		1	1	9.36E+04	9.74E+04	-0.058		2	GPI transamidase component PIG-S
Q9UBV2	SE1L1_HUMAN	SEL1L		4	4	4.69E+05	4.84E+05	-0.046	Y	1	Protein sel-1 homolog 1
Q92896	GSLG1_HUMAN	GLG1		4	4	1.20E+06	1.24E+06	-0.044		1	Golgi apparatus protein 1
P51788	CLCN2_HUMAN	CLCN2		1	1	1.16E+05	1.19E+05	-0.037	Y	12	Chloride channel protein 2
O15393	TMPS2_HUMAN	TMPRSS2		1	1	1.90E+04	1.93E+04	-0.020	Y	1	Transmembrane protease serine 2
Q9HD43	PTPRH_HUMAN	PTPRH		5	5	7.18E+05	7.19E+05	-0.001	Y	1	Receptor-type tyrosine-protein phosphatase H
Q9UBS9	CA009_HUMAN	C1orf9		1	1	1.54E+03	1.54E+03	0.006		1	Protein C1orf9
Q9HD45	TM9S3_HUMAN	TM9SF3		2	2	7.88E+06	7.64E+06	0.044	Y	9	Transmembrane 9 superfamily member 3
Q9UHN6	TMEM2_HUMAN	TMEM2		6	5	2.01E+05	1.93E+05	0.055	Y	1	Transmembrane protein 2
Q04912	RON_HUMAN	MST1R	CD136	4	3	1.94E+05	1.86E+05	0.056	Y	1	Macrophage-stimulating protein receptor
Q13433	S39A6_HUMAN	SLC39A6		2	2	5.77E+04	5.54E+04	0.057	Y	6	Zinc transporter ZIP6
Q14573	ITPR3_HUMAN	ITPR3		2	2	4.73E+04	4.52E+04	0.065		7	Inositol 1,4,5-trisphosphate receptor type 3
Q9HAW8	UD110_HUMAN	UGT1A10		6	6	8.58E+05	8.15E+05	0.075		1	UDP-glucuronosyltransferase 1-10
P12259	FA5_HUMAN	F5		2	2	5.71E+04	5.42E+04	0.077		0	Coagulation factor V
Q9UNP4	SIAT9_HUMAN	ST3GAL5		1	1	1.48E+04	1.40E+04	0.080	Y	1	Lactosylceramide alpha-2,3-sialyltransferase
P13473	LAMP2_HUMAN	LAMP2	CD107b	6	5	1.73E+05	1.62E+05	0.088	Y	1	Lysosome-associated membrane glycoprotein 2
P11166	GTR1_HUMAN	SLC2A1		4	4	4.92E+06	4.61E+06	0.095	Y	12	Solute carrier family 2, facilitated glucose transporter member 1
P21583	SCF_HUMAN	KITLG		1	1	1.23E+04	1.15E+04	0.103	Y	1	Kit ligand
Q8N8Z6	DCBD1_HUMAN	DCBLD1		1	1	3.17E+04	2.94E+04	0.110	Y	1	Discoidin, CUB and LCCL domain-containing protein 1
P13987	CD59_HUMAN	CD59	CD59	1	1	3.84E+04	3.55E+04	0.116		GPI	CD59 glycoprotein
Q969P0	IGSF8_HUMAN	IGSF8	CD316	1	1	9.09E+03	8.26E+03	0.138	Y	1	Immunoglobulin superfamily member 8

O43688	LPP2_HUMAN	PPAP2C		1	1	8.51E+04	7.71E+04	0.142	Y	6	Lipid phosphate phosphohydrolase 2
P55011	S12A2_HUMAN	SLC12A2		1	1	7.98E+05	7.20E+05	0.149	Y	12	Solute carrier family 12 member 2
O75144	ICOSL_HUMAN	ICOSLG	CD275	1	1	4.64E+04	4.18E+04	0.152	Y	1	ICOS ligand
Q6PIU2	NCEH1_HUMAN	NCEH1		3	3	2.49E+05	2.22E+05	0.169		0	Neutral cholesterol ester hydrolase 1
Q9H0X4	ITFG3_HUMAN	ITFG3		3	3	6.16E+05	5.44E+05	0.179		1	Protein ITFG3
Q7KYR7	BT2A1_HUMAN	BTN2A1		1	1	1.47E+04	1.28E+04	0.191	Y	1	Butyrophilin subfamily 2 member A1
P52799	EFNB2_HUMAN	EFNB2		1	1	2.47E+04	2.15E+04	0.199	Y	1	Ephrin-B2
P12830	CADH1_HUMAN	CDH1	CD324	4	4	5.59E+05	4.80E+05	0.221	Y	1	Cadherin-1
Q14126	DSG2_HUMAN	DSG2		7	7	1.45E+06	1.24E+06	0.221		1	Desmoglein-2
Q9NTN9	SEM4G_HUMAN	SEMA4G		1	1	1.23E+04	1.06E+04	0.221	Y	1	Semaphorin-4G
P05362	ICAM1_HUMAN	ICAM1	CD54	4	4	9.49E+05	8.06E+05	0.236	Y	1	Intercellular adhesion molecule 1
P40189	IL6RB_HUMAN	IL6ST	CD130	5	5	2.56E+05	2.16E+05	0.249	Y	1	Interleukin-6 receptor subunit beta
Q15043	S39AE_HUMAN	SLC39A14		1	1	1.44E+05	1.19E+05	0.272	Y	6	Zinc transporter ZIP14
Q15165	PON2_HUMAN	PON2		3	3	1.76E+05	1.45E+05	0.279		0	Serum paraoxonase\arylesterase 2
O60635	TSN1_HUMAN	TSPAN1		2	2	1.08E+05	8.78E+04	0.295	Y	4	Tetraspanin-1
P16278	BGAL_HUMAN	GLB1		5	5	2.15E+05	1.73E+05	0.309		0	Beta-galactosidase
Q13641	TPBG_HUMAN	TPBG		5	5	8.75E+05	7.04E+05	0.314	Y	1	Trophoblast glycoprotein
Q5NDL2	AER61_HUMAN	AER61		1	1	9.45E+03	7.54E+03	0.327		0	Uncharacterized glycosyltransferase AER61
Q12797	ASPH_HUMAN	ASPH		2	2	1.12E+06	8.53E+05	0.388		1	Aspartyl\asparaginyl beta-hydroxylase
Q969V3	NCLN_HUMAN	NCLN		1	1	1.17E+05	8.97E+04	0.389	Y	2	Nicalin
Q9Y487	VPP2_HUMAN	ATP6V0A2		2	2	3.26E+04	2.45E+04	0.412	Y	8	V-type proton ATPase 116 kDa subunit a isoform 2
P26006	ITA3_HUMAN	ITGA3	CD49c	8	7	1.25E+06	9.31E+05	0.424	Y	1	Integrin alpha-3
O15118	NPC1_HUMAN	NPC1		4	4	1.95E+05	1.45E+05	0.432		13	Niemann-Pick C1 protein
P16422	EPCAM_HUMAN	EPCAM	CD326	10	10	4.64E+06	3.40E+06	0.450		1	Epithelial cell adhesion molecule
Q9Y6H6	KCNE3_HUMAN	KCNE3		1	1	3.59E+04	2.60E+04	0.465	Y	1	Potassium voltage-gated channel subfamily E member 3
P07711	CATL1_HUMAN	CTSL1		1	1	2.03E+04	1.46E+04	0.481		0	Cathepsin L1
O14672	ADA10_HUMAN	ADAM10	CD156c	3	3	1.19E+06	8.53E+05	0.483	Y	1	Disintegrin and metalloproteinase domain-containing protein 10
Q8IWB1	IPRI_HUMAN	ITPRIP		1	1	3.25E+04	2.30E+04	0.497		0	Inositol 1,4,5-triphosphate receptor-interacting protein
Q14002	CEAM7_HUMAN	CEACAM7		2	2	5.70E+04	4.03E+04	0.498		1, GPI	Carcinoembryonic antigen-related cell adhesion molecule 7
P18564	ITB6_HUMAN	ITGB6		1	1	2.55E+04	1.80E+04	0.504	Y	1	Integrin beta-6

Q5T3F8	TM63B_HUMAN	TMEM63B		1	1	1.00E+04	7.04E+03	0.507	Y	11	Transmembrane protein 63B
Q9Y6M7	S4A7_HUMAN	SLC4A7		2	2	8.51E+04	5.85E+04	0.540	Y	11	Sodium bicarbonate cotransporter 3
O43921	EFNA2_HUMAN	EFNA2		2	1	9.03E+04	6.20E+04	0.542		GPI	Ephrin-A2
P29323	EPHB2_HUMAN	EPHB2		1	1	1.07E+05	7.24E+04	0.569	Y	1	Ephrin type-B receptor 2
Q9P2B2	FPRP_HUMAN	PTGFRN	CD315	7	7	9.78E+05	6.48E+05	0.594	Y	1	Prostaglandin F2 receptor negative regulator
P16144	ITB4_HUMAN	ITGB4	CD104	8	8	1.53E+06	1.01E+06	0.595		1	Integrin beta-4
Q8NC42	RN149_HUMAN	RNF149		1	1	5.25E+04	3.47E+04	0.597	Y	1	E3 ubiquitin-protein ligase RNF149
Q96PB1	CASD1_HUMAN	CASD1		2	2	3.56E+04	2.32E+04	0.618	Y	14	CAS1 domain-containing protein 1
Q6P9F7	LRC8B_HUMAN	LRRC8B		1	1	2.57E+04	1.67E+04	0.626	Y	4	Leucine-rich repeat-containing protein 8B
Q02487	DSC2_HUMAN	DSC2		1	1	1.21E+05	7.71E+04	0.645		1	Desmocollin-2
Q9NUM4	T106B_HUMAN	TMEM106B		2	2	3.40E+04	2.17E+04	0.648	Y	1	Transmembrane protein 106B
O75054	IGSF3_HUMAN	IGSF3		5	5	8.01E+05	5.08E+05	0.657	Y	1	Immunoglobulin superfamily member 3
Q58DX5	NADL2_HUMAN	NAALADL2		1	1	2.14E+04	1.34E+04	0.680	Y	1	Inactive N-acetylated-alpha-linked acidic dipeptidase-like protein 2
Q92485	ASM3B_HUMAN	SMPDL3B		1	1	2.36E+03	1.48E+03	0.680		0	Acid sphingomyelinase-like phosphodiesterase 3b
Q9H5V8	CDCP1_HUMAN	CDCP1	CD318	4	4	1.97E+05	1.22E+05	0.692	Y	1	CUB domain-containing protein 1
Q96AP7	ESAM_HUMAN	ESAM		1	1	3.19E+04	1.92E+04	0.730	Y	1	Endothelial cell-selective adhesion molecule
Q29983	MICA_HUMAN	MICA		2	1	2.49E+04	1.50E+04	0.731	Y	1	MHC class I polypeptide-related sequence A
O60779	S19A2_HUMAN	SLC19A2		1	1	2.05E+05	1.24E+05	0.733	Y	12	Thiamine transporter 1
P21709	EPHA1_HUMAN	EPHA1		3	3	1.72E+05	1.00E+05	0.786	Y	1	Ephrin type-A receptor 1
P16070	CD44_HUMAN	CD44	CD44	4	3	3.11E+06	1.80E+06	0.791	Y	1	CD44 antigen
Q96K49	TM87B_HUMAN	TMEM87B		2	2	1.61E+05	9.31E+04	0.791	Y	7	Transmembrane protein 87B
Q53GD3	CTL4_HUMAN	SLC44A4		1	1	5.30E+03	3.03E+03	0.805	Y	10	Choline transporter-like protein 4
Q14118	DAG1_HUMAN	DAG1		2	1	3.34E+04	1.89E+04	0.824	Y	1	Dystroglycan
P06865	HEXA_HUMAN	HEXA		1	1	4.64E+04	2.57E+04	0.854		0	Beta-hexosaminidase subunit alpha
Q3MIR4	CC50B_HUMAN	TMEM30B		4	4	9.93E+04	5.16E+04	0.945	Y	2	Cell cycle control protein 50B
Q9HDC9	APMAP_HUMAN	APMAP		4	4	6.31E+05	3.24E+05	0.963		1	Adipocyte plasma membrane-associated protein
Q9Y4L1	HYOU1_HUMAN	HYOU1		14	13	6.42E+06	3.27E+06	0.972		0	Hypoxia up-regulated protein 1
Q92854	SEM4D_HUMAN	SEMA4D	CD100	4	3	1.46E+05	7.44E+04	0.973	Y	1	Semaphorin-4D
P13866	SC5A1_HUMAN	SLC5A1		1	1	1.78E+05	9.05E+04	0.978	Y	14	Sodium\glucose cotransporter 1
Q68CR1	SE1L3_HUMAN	SEL1L3		2	2	2.86E+04	1.44E+04	0.992		1	Protein sel-1 homolog 3

Q9H8M5	CNNM2_HUMAN	CNNM2		2	2	3.86E+04	1.91E+04	1.013	Y	4	Metal transporter CNNM2
Q5JRA6	MIA3_HUMAN	MIA3		5	5	2.32E+05	1.15E+05	1.014		2	Melanoma inhibitory activity protein 3
P06756	ITAV_HUMAN	ITGAV	CD51	9	9	4.87E+06	2.37E+06	1.041	Y	1	Integrin alpha-V
Q9Y2B1	TMEM5_HUMAN	TMEM5		1	1	3.85E+04	1.87E+04	1.042		0	Transmembrane protein 5
P35052	GPC1_HUMAN	GPC1		1	1	1.25E+04	5.99E+03	1.058		1, GPI	Glypican-1
Q01973	ROR1_HUMAN	ROR1		1	1	4.32E+03	2.06E+03	1.068	Y	2	Tyrosine-protein kinase transmembrane receptor ROR1
O95858	TSN15_HUMAN	TSPAN15		2	2	2.13E+05	9.86E+04	1.109	Y	5	Tetraspanin-15
Q12866	MERTK_HUMAN	MERTK		2	1	1.10E+04	4.90E+03	1.170	Y	1	Tyrosine-protein kinase Mer
Q08722	CD47_HUMAN	CD47	CD47	2	2	1.38E+05	6.08E+04	1.184	Y	5	Leukocyte surface antigen CD47
O43157	PLXB1_HUMAN	PLXNB1		1	1	1.78E+05	7.67E+04	1.214		1	Plexin-B1
Q99571	P2RX4_HUMAN	P2RX4		1	1	9.74E+03	4.16E+03	1.227	Y	2	P2X purinoceptor 4
O60487	MPZL2_HUMAN	MPZL2		1	1	1.83E+05	7.46E+04	1.294		1	Myelin protein zero-like protein 2
Q13444	ADA15_HUMAN	ADAM15		1	1	7.23E+04	2.86E+04	1.336	Y	1	Disintegrin and metalloproteinase domain-containing protein 15
O15031	PLXB2_HUMAN	PLXNB2		14	14	4.53E+06	1.71E+06	1.401		1	Plexin-B2
P10646	TFPI1_HUMAN	TFPI		1	1	5.78E+04	2.14E+04	1.431		0	Tissue factor pathway inhibitor
Q04771	ACVR1_HUMAN	ACVR1		1	1	4.02E+04	1.45E+04	1.474	Y	1	Activin receptor type-1
Q92508	FA38A_HUMAN	FAM38A		1	1	2.13E+05	7.53E+04	1.500	Y	29	Protein FAM38A
Q68D85	YK047_HUMAN			1	1	5.62E+04	1.98E+04	1.505			Putative Ig-like domain-containing protein DKFZp686O24166\DKFZp686I21167 SV=1
P23229	ITA6_HUMAN	ITGA6	CD49f	10	10	6.26E+06	2.17E+06	1.530	Y	1	Integrin alpha-6
P19256	LFA3_HUMAN	CD58	CD58	3	3	7.16E+05	2.47E+05	1.539	Y	1, GPI	Lymphocyte function-associated antigen 3
Q07954	LRP1_HUMAN	LRP1	CD91	9	9	4.27E+05	1.43E+05	1.581	Y	1	Prolow-density lipoprotein receptor-related protein 1
Q6UXD5	SE6L2_HUMAN	SEZ6L2		3	3	2.87E+05	9.53E+04	1.589	Y	1	Seizure 6-like protein 2
P16444	DPEP1_HUMAN	DPEP1		2	2	4.89E+04	1.57E+04	1.639		1, GPI	Dipeptidase 1
O43490	PROM1_HUMAN	PROM1	CD133	7	7	9.93E+05	3.17E+05	1.646	Y	5	Prominin-1
Q8WTV0	SCRB1_HUMAN	SCARB1		1	1	4.32E+04	1.31E+04	1.727	Y	1	Scavenger receptor class B member 1
P43308	SSRB_HUMAN	SSR2		2	2	4.24E+04	1.28E+04	1.733		1	Translocon-associated protein subunit beta
P48960	CD97_HUMAN	CD97	CD97	2	2	7.63E+04	2.18E+04	1.805	Y	7	CD97 antigen
Q99988	GDF15_HUMAN	GDF15		1	1	1.27E+05	3.60E+04	1.815		0	Growth\differentiation factor 15
P35527	K1C9_HUMAN	KRT9		1	1	7.91E+03	1.93E+03	2.034		0	Keratin, type I cytoskeletal 9
P08174	DAF_HUMAN	CD55	CD55	1	1	1.31E+05	3.02E+04	2.117		GPI	Complement decay-accelerating factor

Q13740	CD166_HUMAN	ALCAM	CD166	5	5	1.73E+06	3.95E+05	2.135	Y	1	CD166 antigen
Q13308	PTK7_HUMAN	PTK7		1	1	5.95E+04	1.30E+04	2.193	Y	1	Tyrosine-protein kinase-like 7
P07942	LAMB1_HUMAN	LAMB1		4	4	1.00E+05	2.14E+04	2.233		0	Laminin subunit beta-1
Q9Y4D7	PLXD1_HUMAN	PLXND1		1	1	5.87E+04	1.25E+04	2.236	Y	1	Plexin-D1
O60637	TSN3_HUMAN	TSPAN3		1	1	1.95E+04	3.70E+03	2.399	Y	4	Tetraspanin-3
P33527	MRP1_HUMAN	ABCC1		4	4	4.54E+05	8.36E+04	2.441	Y	16	Multidrug resistance-associated protein 1
Q9Y5L3	ENTP2_HUMAN	ENTPD2		2	2	3.00E+05	5.35E+04	2.485	Y	1	Ectonucleoside triphosphate diphosphohydrolase 2
P15260	INGR1_HUMAN	IFNGR1	CD119	1	1	3.04E+03	5.01E+02	2.602	Y	1	Interferon gamma receptor 1
Q08174	PCDH1_HUMAN	PCDH1		1	1	8.03E+04	1.22E+04	2.720	Y	1	Protocadherin-1
Q8N4M1	CTL3_HUMAN	SLC44A3		1	1	1.16E+04	1.65E+03	2.814	Y	9	Choline transporter-like protein 3
P10909	CLUS_HUMAN	CLU		2	2	2.11E+05	2.66E+04	2.986		0	Clusterin
Q6UVK1	CSPG4_HUMAN	CSPG4		1	1	2.86E+05	3.20E+04	3.161	Y	1	Chondroitin sulfate proteoglycan 4
P19075	TSN8_HUMAN	TSPAN8		4	4	3.40E+07	3.57E+06	3.251	Y	4	Tetraspanin-8
O43278	SPIT1_HUMAN	SPINT1		2	2	2.19E+05	2.29E+04	3.257	Y	1	Kunitz-type protease inhibitor 1
P06213	INSR_HUMAN	INSR	CD220	3	3	1.60E+05	1.53E+04	3.382	Y	1	Insulin receptor
Q15155	NOMO1_HUMAN	NOMO1		2	1	6.01E+04	5.21E+03	3.527		1	Nodal modulator 1
P78504	JAG1_HUMAN	JAG1	CD339	1	1	2.01E+05	1.61E+04	3.642	Y	1	Protein jagged-1
P27487	DPP4_HUMAN	DPP4	CD26	4	4	1.04E+05	8.02E+03	3.702		0	Dipeptidyl peptidase 4
Q9UM44	HHLA2_HUMAN	HHLA2		1	1	9.07E+04	6.60E+03	3.780	Y	1	HERV-H LTR-associating protein 2
O43570	CAH12_HUMAN	CA12		4	4	1.23E+06	6.84E+04	4.165	Y	1	Carbonic anhydrase 12
P98088	MUC5A_HUMAN	MUC5AC		2	2	8.05E+04	4.07E+03	4.304		0	Mucin-5AC (Fragments)
P13726	TF_HUMAN	F3	CD142	1	1	5.34E+04	1.26E+03	5.407	Y	1, GPI	Tissue factor
P06731	CEAM5_HUMAN	CEACAM5	CD66e	6	6	2.47E+06	1.75E+04	7.145		1, GPI	Carcinoembryonic antigen-related cell adhesion molecule 5
Q96J84	KIRR1_HUMAN	KIRREL		1	1	2.47E+04	3.22E+01	9.583	Y	1	Kin of IRRE-like protein 1

Supplementary Table 2: Primers sequence for qRT-PCR

Gene	Forward primer	Reverse primer
CAXII	CCACACGACGGGTACTTCTT	AAAGGAACAGCCTTCCAGC
Pgp	ATTCCTCGAGAAACTGCGAA	CACTTCAGGAAGCAACCAG
HIF-1α	TGGCTGCATCTCGAGACTTT	GAAGACATCGCGGGGAC
GLUT1	CCTGCAGTTTGGCTACAACA	TAACGAAAAGGCCCACAGAG
HK	AGACGCACCCACAGTATTCC	CGCATCCTCTTCTTCACCTC
ALDO-A	GCTATGGCCTTTTCCTTTCC	ATGCTCCCAGTGGACTCATC
GAPDH	GAAGGTGAAGGTCGGAGT	CATGGTGGAATCATATTGGAA
PGK	TCTCATGGATGAGGTGGTGA	CTTCCAGGAGCTCCAAACTG
ENO-A	GCTCCGGGACAATGATAAGA	TCCATCCATCTCGATCATCA
LDH	TGGGAGTTCACCCATTAAGC	AGCACTCTCAACCACCTGCT
VEGF	ATCTTCAAGCCATCCTGTGTGC	GCTCACCGCCTCGGCTTGT
EPO	CAGACTTCTACGGCCTGCTG	GCTGAACACTGCAGCTTGAA
CAIX	GTCTCGCTTGGAAGAAATCG	AGAGGGTGTGGAGCTGCTTA
S14	CGAGGCTGATGACCTGTTCT	GCCCTCTCCCACTCTCTCTT